

Processes driving intraseasonal displacements of the eastern edge of the warm pool: the contribution of westerly wind events

Kyla Drushka · Hugo Bellenger · Eric Guilyardi ·
Matthieu Lengaigne · Jérôme Vialard · Gurvan Madec

Received: 14 August 2013 / Accepted: 10 August 2014 / Published online: 3 September 2014
© Springer-Verlag Berlin Heidelberg 2014

Abstract We investigate the processes responsible for the intraseasonal displacements of the eastern edge of the western Pacific warm pool (WPEE), which appear to play a role in the onset and development of El Niño events. We use 25 years of output from an ocean general circulation model experiment that is able to accurately capture the observed displacements of the WPEE, sea level anomalies, and upper ocean zonal currents at intraseasonal time scales in the western and central Pacific Ocean. Our results confirm that WPEE displacements driven by westerly wind events (WWEs) are largely controlled by zonal advection. This paper has also two novel findings: first, the zonal current anomalies responsible for the WPEE advection are driven primarily by local wind stress anomalies and not by intraseasonal wind-forced Kelvin waves as has been shown in most previous studies. Second, we find that intraseasonal WPEE fluctuations that are not related to WWEs are generally caused by intraseasonal variations in net heat flux, in contrast to interannual WPEE displacements that are largely driven by zonal advection. This study hence raises

an interesting question: can surface heat flux-induced zonal WPEE motions contribute to El Niño–Southern Oscillation evolution, as WWEs have been shown to be able to do?

Keywords Westerly wind events · Western Pacific warm pool · Air–sea interaction · El Niño · Intraseasonal variability

1 Introduction

1.1 Importance of the warm pool eastern edge

The western Pacific warm pool is an important component of the global climate system. It is closely associated with the heat source that drives the largest atmospheric circulation cell on earth: the Walker circulation. Sea surface temperatures (SSTs) in the western Pacific are warm, exceeding the necessary threshold for deep atmospheric convection (e.g., Graham and Barnett 1987), which provides a mid-tropospheric heat source in the western Pacific. This drives the Walker circulation: lower tropospheric easterlies in the eastern and central Pacific, with a westerly return flow at height (e.g., Gill 1980). The Walker circulation is associated with a positive feedback called the Bjerknes feedback, in which easterly wind stress in the equatorial western Pacific strengthens the zonal SST gradient, which in turn strengthens the wind stress (Bjerknes 1969). The eastward expansion of the warm pool is thus key to triggering the Bjerknes feedback and inducing the large-scale oceanic and atmospheric anomalies that define El Niño events (e.g., Picaut et al. 1997). This motivates the present study, which aims to understand the dynamics of eastward displacements of the warm pool.

Electronic supplementary material The online version of this article (doi:10.1007/s00382-014-2297-z) contains supplementary material, which is available to authorized users.

K. Drushka (✉) · H. Bellenger · E. Guilyardi · M. Lengaigne ·
J. Vialard · G. Madec
Laboratoire d’Océanographie Expérimentation et Approches
Numériques, CNRS, IRD, MNHN, UPMC, Case 100,
Place Jussieu, 75252 Paris Cedex 05, France
e-mail: kdrushka@apl.uw.edu

Present Address:

K. Drushka
Applied Physics Laboratory, University of Washington, Seattle,
WA, USA

1.2 Interannual variations of the WPEE

Interannual zonal warm pool eastern edge (WPEE) displacements are thought to be crucial in the genesis of El Niño events (Wang and Picaut 2004) and a fundamental cause of remote responses to El Niño–Southern Oscillation (ENSO) through atmospheric teleconnections (e.g., Trenberth et al. 1998; Ashok et al. 2007). In the eastern Pacific, the main driver of interannual SST variations is vertical exchanges with the subsurface (vertical mixing, entrainment and upwelling modulation): remote central Pacific forcing modulates the depth of the thermocline, and thus the amount of cold upwelling, in the eastern Pacific (Zhang and McPhaden 2006). In contrast, SST changes in the western and central Pacific Ocean are dominated by zonal advection arising from low-frequency currents (Vialard and Delecluse 1998; Vialard et al. 2001). Zonal heat advection also appears to drive interannual variations in the position of the WPEE (Picaut et al. 1996, 2001; Vialard et al. 2001).

1.3 Influence of intraseasonal variations on ENSO

In addition to interannual variations, energetic intraseasonal variations occur in the western Pacific. At lower intraseasonal frequencies (roughly 30–100 days), these variations are often associated with the Madden-Julian Oscillation (MJO; see Zhang 2005, for a review). The MJO is a system of coupled large-scale anomalies in convection and winds that originates in the Indian Ocean and travels eastward to the western Pacific, modulating the surface momentum and heat fluxes. At higher frequencies within the intraseasonal band, westerly wind events (WWEs, also called westerly wind bursts) frequently occur in the western equatorial Pacific (see Lengaigne et al. 2004a, for a review). The precise definition of WWEs varies, but they are typically defined as having zonal scales of tens of degrees longitude and persisting for several days or more (e.g., Harrison and Vecchi 1997; Seiki and Takayabu 2007). WWEs, which occur preferentially during boreal autumn and winter, are thought to be excited by active phases of the MJO (e.g., Zhang 2005), tropical cyclones (e.g., Keen 1982), cold surges from midlatitudes (e.g., Harrison 1984), or a combination of these processes (Yu and Rienecker 1998). In addition, the observed probability of occurrence of these WWEs depends on ENSO-related background SST (Yu et al. 2003; Tziperman and Yu 2007; Seiki and Takayabu 2007), WWEs being three times more likely to occur when the eastern edge of the warm pool is located to the east of the date line (Eisenman et al. 2005). Such WWEs can induce coupled ocean–atmosphere responses, which modulate the strength or

timing of El Niño events (Gebbie and Tziperman 2009) and contribute to the irregularity and diversity of ENSO characteristics (Gebbie et al. 2007; Lopez and Kirtman 2013; Lopez et al. 2013; Fedorov et al. 2014). WWEs can force oceanic Kelvin waves that advect the WPEE eastward and deepen the thermocline in the eastern Pacific Ocean (Boulangier and Menkes 1999; Lengaigne et al. 2002). As a consequence of the WWE state-dependency, eastward warm pool displacement allows subsequent WWEs to occur further east, inducing a progressive WPEE eastward displacement (McPhaden 1999; Lengaigne et al. 2003a, 2004b), which favors the onset and development of an El Niño event.

Similarly, a secondary westerly wind anomaly could be generated locally by the anomalously warm SSTs, a mechanism consistent with the observed evidence that WWE occurrence is modulated by the background SST (Yu et al. 2003; Tziperman and Yu 2007; Seiki and Takayabu 2007). For instance, Tziperman and Yu (2007) used satellite observations to demonstrate that the large-scale Pacific Ocean SST structure affects the probability of occurrence, amplitude, location, and scale of WWEs. Similarly, Latif et al. (1988); Lengaigne et al. (2003a, 2004b) used sensitivity tests with atmospheric and coupled general circulation models to demonstrate that a SST increase following a WWE causes an eastward shift of the ascending branch of the Walker circulation, which produces enhanced westerly wind activity following the initial westerly wind event. Results from these studies and others therefore suggests that WWE-related warming at the WPEE can induce subsequent WWEs via air–sea coupling. The present study supports the idea that coupled feedbacks between SST and WWEs are integral to ENSO dynamics (Gebbie et al. 2007; Lopez and Kirtman 2013; Fedorov et al. 2014).

1.4 Previous studies of intraseasonal SST variations in the Pacific

Many studies have investigated the intraseasonal oceanic variability in the equatorial Pacific (see Kessler 2005, for a review). This is a difficult task in the eastern Pacific, where instabilities in the equatorial current systems known as tropical instability waves (TIWs) or Legeckis waves (Legeckis 1977) are an energetic source of intraseasonal variations (e.g., Qiao and Weisberg 1995; Farrar 2011), and can obscure intraseasonal Kelvin wave signals. TIWs have considerable impacts on intraseasonal heat and momentum budgets in the eastern Pacific Ocean (Baturin and Niiler 1997; Menkes et al. 2006) and rectify onto seasonal (Im et al. 2012) and interannual scales (e.g., Vialard et al. 2001; Jiang et al. 2009). The intraseasonal heat balance is hence quite complex in the east: vertical advection and entrainment (McPhaden 2002), horizontal advection (Lucas et al.

2010), or a combination of both (Halkides et al. 2011) influence intraseasonal SST variations. In the central Pacific Ocean around the dateline, in the vicinity of the WPEE, anomalous zonal jets act on a strong mean zonal temperature gradient, so zonal heat advection can dominate intraseasonal SST anomalies (Shinoda and Hendon 2001; McPhaden 2002; Matthews et al. 2010; Drushka et al. 2012). Finally, many studies have focused on intraseasonal SST variations associated with the MJO within the warm pool, and it is well demonstrated that they are dominated by heat flux anomalies at the air–sea interface (Hendon and Glick 1997; Shinoda et al. 1998; McPhaden 2002).

While the eastern, western and central Pacific Ocean intraseasonal SST budgets have been thoroughly quantified in the past, intraseasonal temperature variations right at the WPEE have not been well documented. The position of the WPEE varies widely, from around 140° E during La Niña events to the far eastern Pacific in the case of extreme El Niño events (e.g., Maes et al. 2010), so depending on whether the warm pool is confined to the far western Pacific or stretches out toward the eastern part of the basin, different processes may act to produce temperature anomalies at the WPEE. In addition, most studies considering eastward intraseasonal zonal warm pool displacements have focused on the role of wind-forced downwelling Kelvin waves, which excite geostrophic currents that act on the temperature gradient at the WPEE to advect warm water eastward (Kessler et al. 1995; Picaut and Delcroix 1995; Picaut et al. 1996; McPhaden 1999; Delcroix and Dewitte 2000; Lengaigne et al. 2002). However, other thermodynamic processes may also produce intraseasonal displacements of the WPEE. For example, Kessler et al. (1995), in a study of the MJO, pointed out that abrupt shifts in the WPEE are not always associated with Kelvin waves. In addition, sources of momentum other than Kelvin wave-related geostrophic currents may cause heat advection at the WPEE: Boulanger et al. (2001) found that nonlinear interaction between the wind-forced jet and the thermohaline front at the WPEE can contribute substantially to eastward WPEE displacement; Lengaigne et al. (2002) confirmed this result and also showed that salinity anomalies at the WPEE can induce an anomalous zonal pressure gradient that contributes to the eastward jet and thus to warm pool displacement. Feng et al. (2005) showed that the Coriolis term can also contribute significantly to intraseasonal zonal momentum anomalies associated with WWEs. Finally, Boulanger and Menkes (1999) noted that reflected downwelling Rossby waves, propagating westward along the equator, can counter the eastward currents excited by Kelvin waves, halting eastward warm pool displacement.

It hence seems necessary to study the upper ocean intraseasonal heat budget at the WPEE in order to understand the mechanisms controlling its intraseasonal displacements,

which may play a key role in the onset of El Niño events. To our knowledge, this question has not been explicitly addressed: previous studies have only considered intraseasonal upper ocean heat budgets in an Eulerian framework rather than in the Lagrangian frame of the WPEE. In the present study, we use 25 years of output from an ocean general circulation model (OGCM) to examine intraseasonal mixed-layer heat and momentum balances at the WPEE in order to understand what controls the displacement of the warm pool on intraseasonal time scales. In Sect. 2 we introduce the model and the observational datasets used for validation, and in Sect. 3 we compare the model output with the validation datasets. Section 4 discusses the heat and momentum budgets at the WPEE, and Sect. 5 shows these budgets for the cases of WWEs only. The results are summarized and discussed in Sect. 6. We present two novel findings: first, heat fluxes drive intraseasonal excursions of the WPEE while zonal heat advection dominates during westerly wind events; and second, following WWEs, local wind stress is more important for driving zonal surface currents, and thus advection, than are Kelvin waves.

2 Data and methods

2.1 Model setup

The numerical simulation used in this study follows the strategy developed within the DRAKKAR project (Brodeau et al. 2010), and is based on the NEMO (Nucleus for European Modelling of the Ocean) Ocean General Circulation Model (Madec 2008). The model is based on primitive equations, and uses a free surface formulation (Roulet and Madec 2000). Our configuration uses an eddy-permitting 1/4° resolution and 46 vertical levels, with 6-m spacing at the surface increasing to 250-m in the deep ocean. Density is computed from potential temperature, salinity and pressure using the Jackett and McDougall (1995) equation of state. Vertical mixing is parameterized from a turbulence closure scheme based on a prognostic vertical turbulent kinetic equation, which has been shown to perform well in the tropics before (e.g., Blanke and Delecluse 1993; Vialard et al. 2001). Lateral mixing acts along isopycnal surfaces, with a Laplacian operator and 200 m²s⁻¹ constant isopycnal diffusivity coefficient (Lengaigne et al. 2003b). Shortwave fluxes penetrate into the ocean based on a single exponential profile corresponding to oligotrophic water (Paulson and Simpson 1977) with an attenuation depth of 23 m (Lengaigne et al. 2007).

The model was forced from 1979 to 2007 with the DRAKKAR Forcing Set 4.2 (DFS4.2) dataset (Brodeau et al. 2010). This dataset is essentially based on the corrected ERA-40 reanalysis (and ECMWF operational

analyses beyond 2002) for near-surface meteorological variables (Uppala et al. 2005), and on the corrected ISCCP-FD radiation product (Zhang et al. 2004) after 1984. No surface temperature restoring was used; salinity was restored to climatological values, with a relaxation time-scale of 33 days (for a 10 m-thick layer). The model was started from rest, using climatological salinity and temperature from the World Ocean Atlas (Locarnini et al. 2010), and spun up for 5 years using the DFS4.2 forcing. The air temperature and humidity were specified (whereas they adjust to the SST over open ocean in the real world); this is equivalent to a “hidden relaxation”, which can lead to the right SST for the wrong reasons (Boyer et al. 2007). To estimate the amplitude of this hidden relaxation, we also estimated fluxes using the bulk formulae and SSTs from the ERA-40 reanalysis; the difference between the flux values estimated from the bulk formulae and by the model provides an uncertainty on the model surface heat fluxes. We computed the SST tendency corresponding to this term in the surface layer heat budget (see below), and hence provide an error bar on the heat budget.

This model and forcing strategy have been shown to accurately capture interannual variations of the tropical Pacific heat content and SSTs (Lengaigne et al. 2012); decadal variation in the Indo-Pacific sea level (Nidheesh et al. 2012); and interannual (Keerthi et al. 2012) and intraseasonal (Vialard et al. 2012; Nisha et al. 2013) variations of the mixed layer and SST in the Indo-Pacific region.

Daily model outputs on a 0.25° grid were stored. To avoid potential problems arising from the fact that the DFS4.2 forcing set uses climatological shortwave fluxes prior to 1984, we limited the time period of the study to 1984–2008.

2.2 Heat and momentum budgets

The time tendency for temperature (T) averaged over the mixed layer (\mathcal{T} , taken as a proxy for SST) is described (e.g., Vialard et al. 2001) by:

$$\partial_t \mathcal{T} = \underbrace{\frac{Q_s(1-f|_{-h}) + Q^*}{\rho c_p h}}_a - \underbrace{\int_{-h}^0 u \partial_x T dz}_b - \underbrace{\int_{-h}^0 v \partial_y T dz}_c - \underbrace{\left(\frac{(\kappa \partial_z T)|_{-h} + (w|_{-h} + \frac{dh}{dt})(T|_{-h} - \mathcal{T})}{h} + \int_{-h}^0 D(T) dz \right)}_d. \quad (1)$$

The terms on the right-hand side of Eq. 1 are as follows: Q_s and Q^* are the solar and non-solar components of heat flux, and $f|_{-h}$ is the fraction of incoming solar radiation that penetrates deeper than the mixed layer and thus does not contribute to its heating. The heating rate caused by the total heat flux is scaled by the time-varying mixed-layer depth (h)

and the volumetric heat capacity of water (ρc_p) so that term a represents the total heat flux absorbed by the mixed layer. Mixed-layer depth is based on a potential density anomaly of 0.01 kg m^{-3} relative to the surface. Terms b and c represent the zonal and meridional advection of \mathcal{T} . Term d represents horizontal diffusion and vertical processes: κ is the vertical tracer mixing coefficient, so $\kappa \partial_z T|_{-h}$ represents turbulent entrainment. $w|_{-h}(T|_{-h} - \mathcal{T})h^{-1}$ is vertical heat advection into the mixed layer and $\frac{dh}{dt}(T|_{-h} - \mathcal{T})h^{-1}$ is the vertical entrainment of deeper water into the mixed layer, which is computed as the budget residual. Term d is the horizontal diffusion, which is usually negligible in the present analyses.

The zonal momentum budget can be written as:

$$\partial_t u = \frac{1}{\rho} \partial_z \tau^x - \frac{1}{\rho} \partial_x p - (u \partial_x u + v \partial_y u) - w \partial_z u + f v. \quad (2)$$

Here, u is zonal velocity, ρ is seawater density, τ^x is the zonal component of wind stress, p is the pressure, and f is the Coriolis parameter. Each term was averaged over the top 3 model layers (16 m) in order to represent the surface-layer momentum without incorporating exchanges with the subsurface layer (entrainment).

2.3 Observations and reanalysis

In Sect. 3, we validate the model variables that are relevant to this study. We use daily SSTs from the Tropical Rainfall Measuring Mission (TRMM) Microwave Imager (TMI), which are available from 1998 to present on a $0.25^\circ \times 0.25^\circ$ grid. Sea level anomaly (SLA), measured by satellite altimeters, comes from Aviso and is available as a 7-day $\times 0.25^\circ \times 0.25^\circ$ gridded product from October 1992 to present (Ducet et al. 2000). We validate the model heat and momentum flux components against those from TropFlux, a daily, gridded product with 1° horizontal resolution that has been shown to perform at least as well as other commonly-used products in capturing intraseasonal heat and momentum flux anomalies in the tropics (Kumar et al. 2012a, b) and is available from 1979–2012, which includes the entire model run. Finally, we validate the modeled upper ocean currents against in situ observations from the Tropical Atmosphere Ocean (TAO) moorings along the equator, which measured ocean velocities using current meters and/or acoustic Doppler current profilers (ADCPs) (McPhaden et al. 1998). As there are large data gaps in the early part of the TAO time series, we only compare over the time period 1990–2008.

2.4 Filtering and removal of TIW-related signals

This study is focused on equatorial dynamics, so all model outputs were averaged over the latitude band $2^\circ\text{S}–2^\circ\text{N}$. The

equatorially-averaged daily data were then filtered by first removing the seasonal signal (first three harmonics of the annual cycle) and then applying a low-pass filter with a 120-day Hamming window having a half-power frequency of 98 days^{-1} in order to calculate interannual anomalies. By removing the interannual and seasonal signals from the raw data, we obtained a good estimate of intraseasonal anomalies. Fast variations were removed by applying a low-pass filter with a cut-off of 7 days. This filtering essentially consisted of a 7–120-day bandpass, except that the interannual components were specifically retained in order to quantify interannual variations.

Tropical instability waves, though also in the intraseasonal band, have distinctly different properties, causes, and dynamical implications than the eastward-propagating intraseasonal signals originating in the western Pacific that are the focus of the present study (Menkes et al. 2006, and references therein). Here, we do not want to include TIWs in the heat budget analysis so we removed them using a frequency–wavelength decomposition following Farrar (2011): a 2-dimensional fast Fourier transform (FFT) was performed on each of the intraseasonally-bandpassed time series; the edges of the time series were tapered to zero using Tukey windows 154 days and 10° wide, respectively; the westward-propagating (negative wavenumber) components within the 10–40-day, 4° – 25° longitude window were set to zero; and a reverse FFT was performed. Figure 1 illustrates this procedure on the SST field, and shows that it efficiently reduces westward-propagating signals in the eastern Pacific Ocean while retaining the intraseasonal variations that originate in the western Pacific and

propagate eastward along the equator. Note that most TIW activity occurs east of the warm pool, so the filtering does not have substantial impacts on the results near the WPEE.

We decompose each individual term X in Eqs. 1 and 2 into its background (interannual + seasonal) and intraseasonal components in order to estimate the contribution of each to the intraseasonal mixed-layer heat and momentum budget: $X = \bar{X} + X'$, where \bar{X} denotes the background and X' the intraseasonal signal. By keeping only the X' components we can isolate the intraseasonal variations. For example, when applied on the non-linear advection term, this filtering allows all terms contributing to intraseasonal variations to be isolated:

$$-(uT_x)' = -u'\bar{T}_x - \bar{u}T_x' - u'T_x' \quad (3)$$

We hence simply show the intraseasonal heat budget by filtering all the nonlinear terms of the full mixed-layer heat and momentum budget equations. The sensitivity of our findings to the filtering is discussed in Sect. 6.2.

2.5 Warm pool eastern edge definition

Many different definitions of the warm pool have been proposed. These usually rely on identifying the longitude at which the sea surface exceeds a threshold value of temperature (e.g., McPhaden and Picaut 1990), salinity (e.g., Bosc et al. 2009), or ocean color (Maes et al. 2010). Warm SSTs tend to enhance convection (Graham and Barnett 1987), and since the present study is concerned with exchanges of heat at the edge of the warm pool, we rely on a temperature threshold of 29°C to define the WPEE. We explored

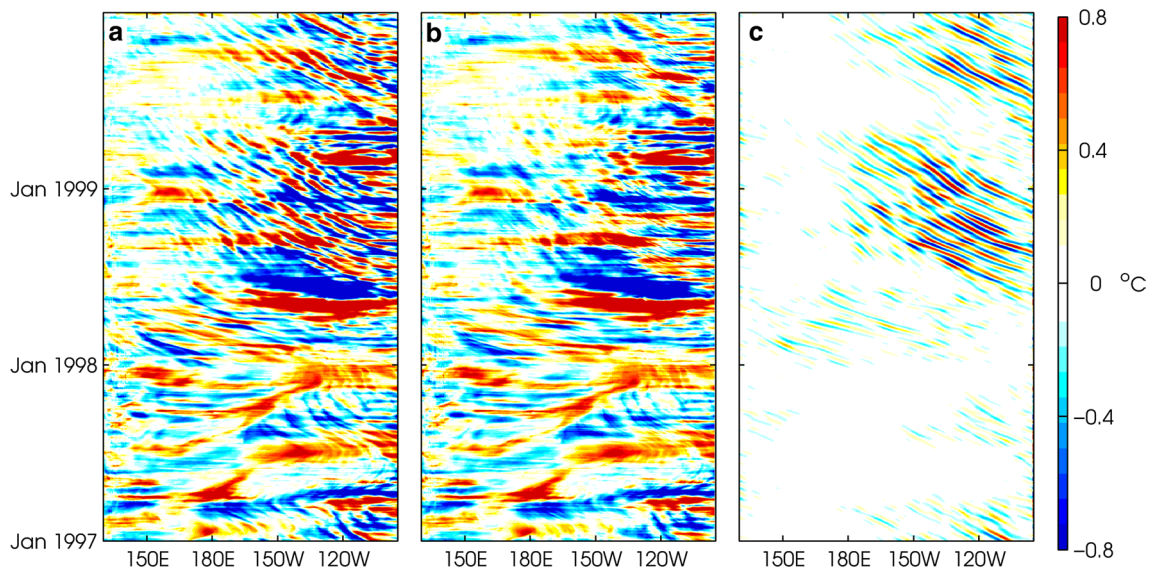


Fig. 1 Example illustrating the filtering used to remove tropical instability waves: **a** equatorially-averaged intraseasonal SST from the model; **b** intraseasonal signal after 2D filtering has been applied to remove TIWs; **c** TIWs removed using 2D filtering (i.e. difference between **a** and **b**)

numerous definitions of the WPEE, including a single isotherm, an average between two isotherms, or an average over longitudes immediately east and west of a single isotherm. We found our results to be robust across a range of WPEE definitions, as will be demonstrated in the discussion section.

2.6 Westerly wind events: definition and statistics

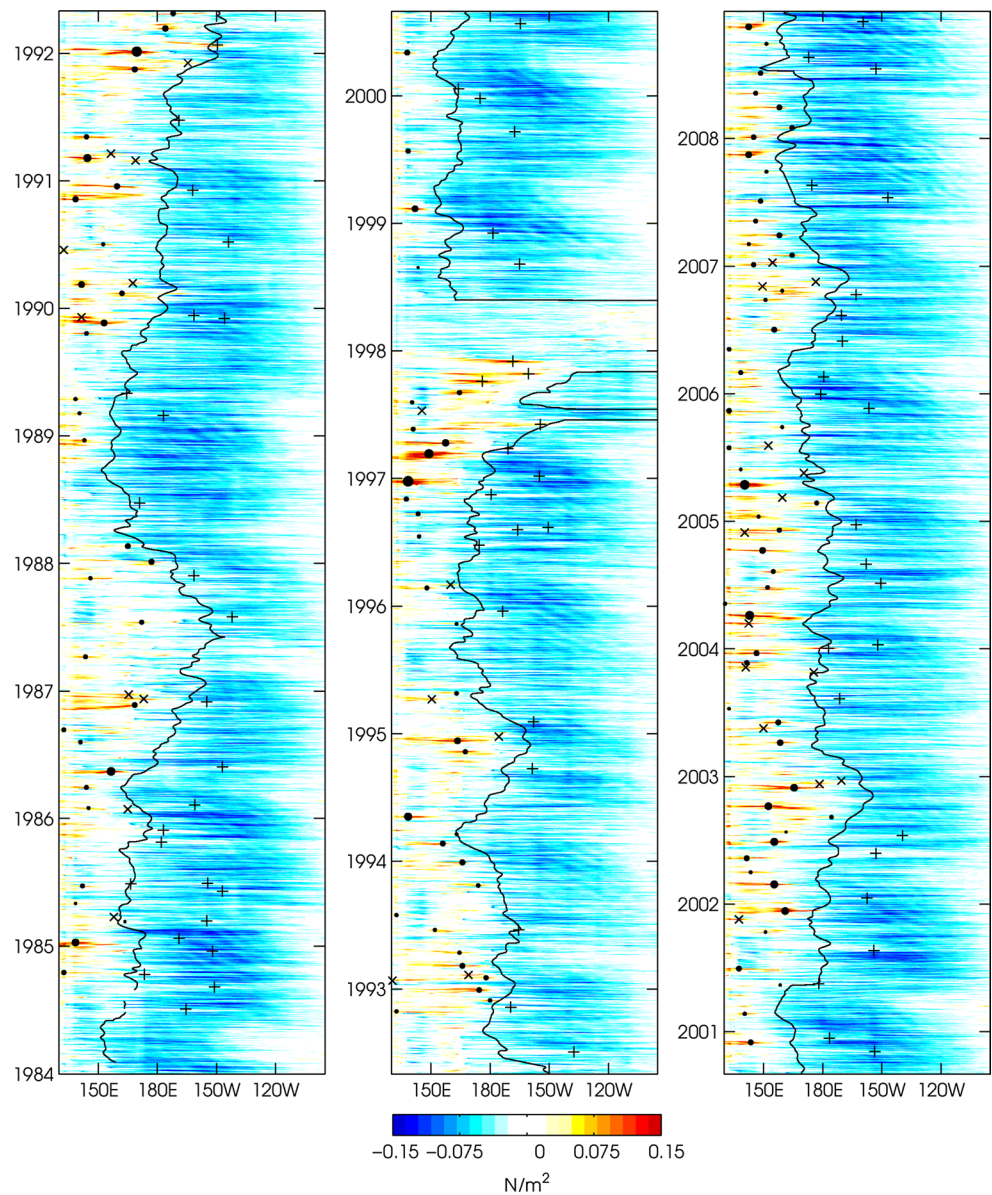
There is no single way to define WWEs. For example, Harrison and Vecchi (1997) looked in 10° latitude \times $\sim 30^\circ$ longitude boxes within the equatorial Pacific Ocean and characterized WWEs based on having zonal wind anomalies exceeding 2 m s^{-1} for at least 3 days. Seiki and Takayabu (2007) averaged zonal winds between 2.5°S and 2.5°N and chose events for which anomalies in zonal wind speed with respect to the mean seasonal cycle exceeded 5 m s^{-1} for at least 10° longitude for at least 2 days. In the present study, we explored many definitions of WWEs, including those of Harrison and Vecchi (1997) and Seiki and Takayabu (2007), and found the qualitative results of the study to be not at all sensitive to the choice. We thus used a particularly stringent definition in order to select only WWEs that are (a) likely to impact the WPEE and the equatorial dynamics, and (b) not likely to be redundant. WWEs were identified using ERA-40 wind stress, the same wind dataset used to force the model. Wind stress observations, averaged over the equatorial wave guide (2°S – 2°N), were filtered as described above to isolate the intraseasonal anomalies, and cases for which zonal wind stress anomaly exceeded 0.035 N m^{-2} (corresponding roughly to 5 m s^{-1}) were extracted; if these patches of wind had a longitudinal extent of at least 10° and persisted for at least 3 days, they were considered to be WWEs. Figure 2 shows unfiltered zonal wind stress over the equatorial Pacific Ocean as well as the time, longitude, and relative amplitude of both the WWEs used in this study and those that were rejected. Over the 1984–2008 period, 216 events met the above criteria. Since we are interested in the impacts of WWEs on the dynamics at the WPEE, we only considered WWEs that occurred within the western Pacific warm pool, that is, west of the WPEE at a given time; this stipulation eliminated 71 WWEs (Fig. 2). Finally, there are a number of cases in which several wind anomalies occur within a short timespan and appear to produce a single Kelvin wave response, and it is impossible to determine with certainty which wind event drives the Kelvin wave. Were these WWEs each considered individually, this would result in an over-weighting of these events in the statistical analyses. We thus imposed a constraint that WWEs considered in this study must be separated by at least 25 days; in cases for which more than one WWE occurs within a 25-day period, we retained the one with the strongest amplitude, resulting in the exclusion

of a further 31 WWEs. The number of WWEs meeting all of these criteria and used in this study was 114. This is many fewer than has been identified in earlier studies (e.g., Harrison and Vecchi 1997; Seiki and Takayabu 2007), primarily because those studies were more concerned about general WWE statistics rather than on the impacts of WWEs on the ocean, which guided some of our choices for restricting selected WWEs. The spatio-temporal distribution of WWEs nonetheless generally resembles that found by Seiki and Takayabu (2007), with more events during boreal winter, an increase and an eastward shift of WWEs during El Niño years following the warm pool displacement (see 1997 for instance) and fewer events during La Niña conditions (e.g. 1998–2001).

To illustrate some of the dynamics associated with WWEs, time-longitude sections of the wind and upper ocean response for a large WWE that preceded and may have triggered the 1997–98 El Niño event (e.g., McPhaden 1999) are shown in Fig. 3. This event is not typical of all WWEs considered in this study, but it is a useful example as it has been previously examined in detail (e.g., Boulanger et al. 2001; Lengaigne et al. 2002). The wind event is seen as a strong anomaly in zonal wind stress that spans $\sim 30^\circ$ of longitude centered at around 150°E and persists for nearly 1 month beginning in early March 1997 (Fig. 3a). The WWE excites a Kelvin wave, which is visible as a $\sim 10 \text{ cm}$ anomaly in sea level that propagates eastward at $\sim 3 \text{ m s}^{-1}$ (Fig. 3b, dashed lines). A zonal surface velocity of up to 0.5 m s^{-1} originates beneath the WWE and propagates eastward along the path of the Kelvin wave (Fig. 3d), suggesting that the Kelvin wave excites at least part of the velocity anomaly. Just where the Kelvin wave intersects the WPEE, a weak westerly wind anomaly appears to strengthen the local eastward current anomaly (Fig. 3a, d).

Directly below the WWE, the sea surface begins to cool within a few days of the wind onset (Fig. 3c). This local WWE-related cooling within the warm pool has been documented in many earlier studies (e.g., McPhaden et al. 1992; Cronin and McPhaden 1997) and is the result of evaporative cooling (McPhaden and Hayes 1991), though in this precise case horizontal advection plays a strong role in the cooling seen over the western Pacific (Lengaigne et al. 2002). East of the WWE, the strongest SST anomaly of over 1°C is seen during early April within 10° longitude of the eastern edge of the warm pool. Boulanger et al. (2001) and Lengaigne et al. (2002) showed that this localized warming peak resulted from the particularly strong zonal current acting on the SST gradient near the WPEE. The warm anomaly follows the WPEE as it shifts eastward during the month of April, illustrating how, when the WPEE is defined by an isotherm, positive SST anomalies at the WPEE cause its displacement eastward.

Fig. 2 Unfiltered wind stress (colors) and WWEs (markers: circles centered on peak wind anomaly indicate each of the WWEs used in this study, with the size of the circle proportional to the maximum wind stress anomaly; times indicate wind events that met the maximum size criteria to be defined as a WWE but occurred too close in time from another event ($N = 31$); and +s indicate wind events that occurred east of the WPEE ($N = 71$). The thick black line denotes the WPEE, defined by the 29°C isotherm. Note that the year labels on the y-axis refer to January 1



3 Model validation

Figure 4a, b shows a Hövmöller diagram of unfiltered SSTs from the model and from TMI as well as the WPEE (defined using the 29°C isotherm). Over the concurrent time period of the model and TMI data (1998–2008), the experiment very accurately reproduces both the phase of unfiltered SSTs (correlations of ~ 0.6 – 0.8 in the western Pacific and 0.85 east of the warm pool; Fig. 4c) and its amplitude (regression coefficient $\kappa \sim 1$ everywhere in Fig. 4d). Amplitudes of intraseasonal variations in SST are somewhat underestimated, especially in the central and western Pacific ($\kappa \sim 0.7$; Fig. 4d), and the phase agreement is lower than for the unfiltered data but is still good, ranging between 0.5 and 0.6 . Since our study focuses on the WPEE,

we also validate the WPEE longitude with observed values (Fig. 4a, b): the model captures the observed displacement of the WPEE very well, both for raw values ($R = 0.97$) and at intraseasonal timescales ($R = 0.91$; Fig. 4e). This gives us confidence in the ability of the model to reproduce intraseasonal ocean dynamics at the WPEE. To illustrate the distinction between WWE and intraseasonal variability, intraseasonal WPEE displacements can be identified as excursions in the intraseasonally-filtered WPEE signal (Fig. 4e): for example, there are around 240 intraseasonal WPEE displacements of at least 2° in longitude. Since we have identified 114 WWEs, this means that around half of intraseasonal WPEE displacements may not be linked to WWEs (noting that this ratio depends on how both WWEs and intraseasonal WPEE excursions are defined). This can

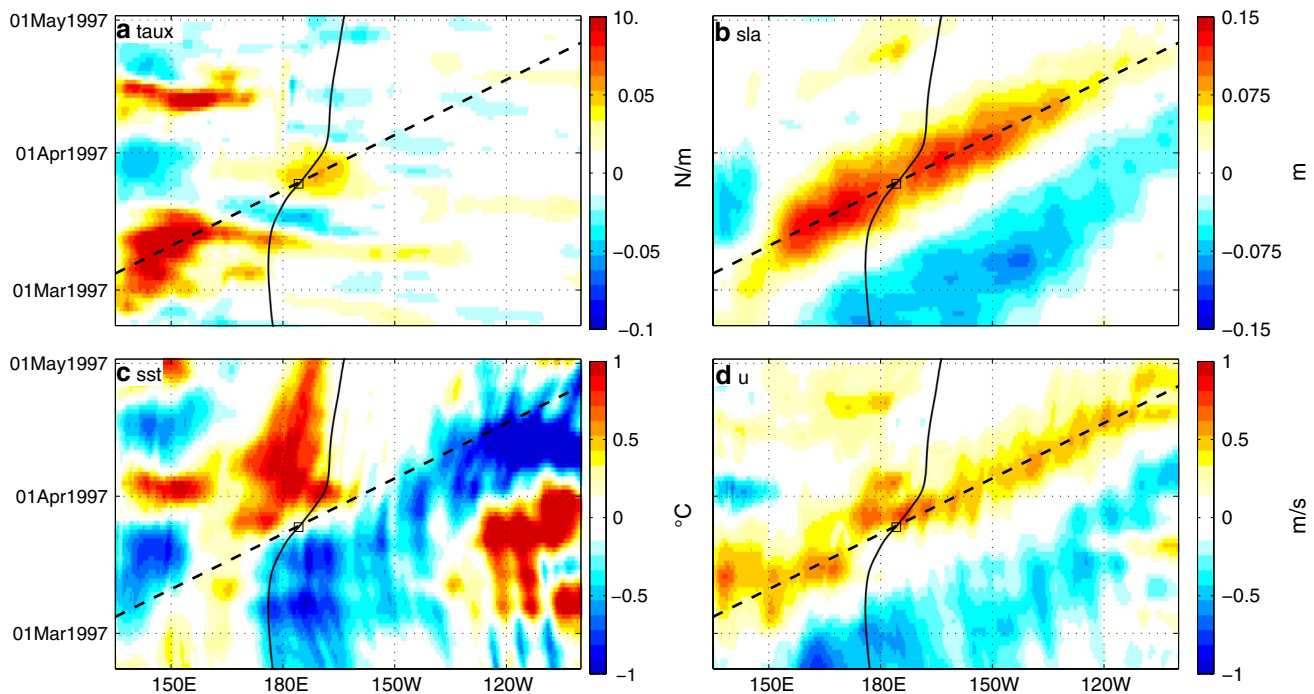


Fig. 3 Equatorially-averaged intraseasonal anomalies associated with a large WWE in March 1997: **a** zonal wind stress; **b** sea level; **c** SST; **d** zonal surface current. In each panel, the WPEE, estimated as the

29°C isotherm, is shown as a *solid black line*; and the Kelvin wave path, inferred from SLA (**b**) is shown as a *dashed black line*. The *square* indicates the intersection of the Kelvin wave and the WPEE

be seen in Fig. 2: for example, the $\sim 10^{\circ}$ eastward WPEE shift in mid-1984 near 155°E that is not preceded by a wind anomaly.

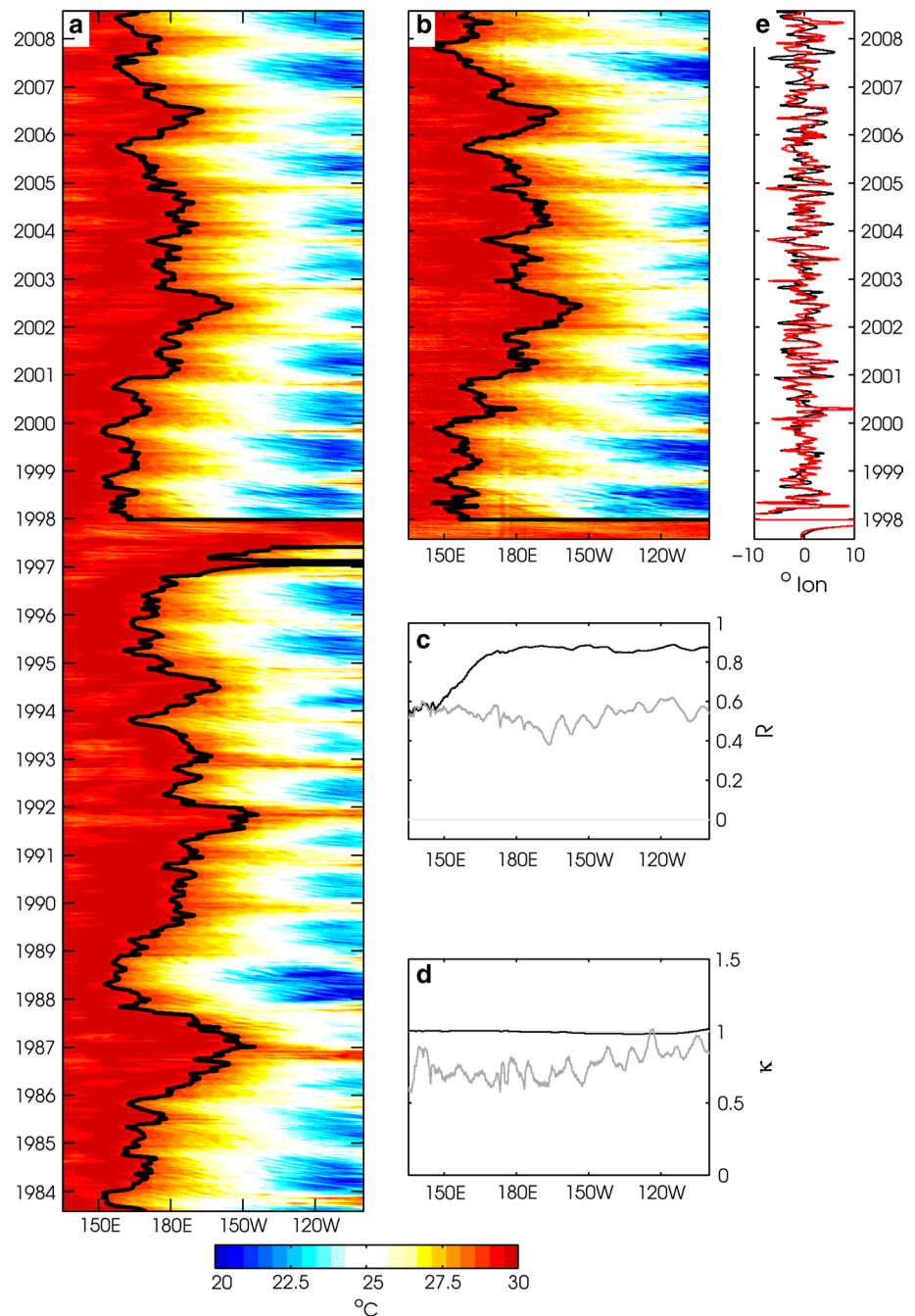
A comparison between modeled and observed intraseasonal SLA is shown in Fig. 5. The daily model output was averaged to 7-day time resolution so as to be comparable with the Aviso SLA product. Over the 1992–2008 time period, the model accurately reproduces the phase and amplitude of unfiltered sea level well ($R \sim 0.8$ and $\kappa > 0.9$, Fig. 5c, d). A comparison of the intraseasonal signal illustrates that the model also reproduces Kelvin waves well: correlations are lowest within the warm pool, where Kelvin waves are weak (Fig. 5a, b) and increase east of the WPEE (Fig. 5c). Most importantly, right at the WPEE, $R = 0.85$ and $\kappa = 0.92$, indicating that the phasing of modeled Kelvin waves at the WPEE is well captured, though the modeled intraseasonal SLAs are underestimated by around 8 %.

We validated the model heat flux components against those from the TropFlux product by comparing the values at the longitude of the WPEE at each time step, over the common time period of 1984–2008. TropFlux intraseasonal shortwave and latent heat fluxes, which dominate the variability at the WPEE (31 and 66 % of the net, respectively) are well correlated with the model values ($R \geq 0.8$; Table 1). Both the model and TropFlux rely on ISCCP shortwave radiation so it is unsurprising that they are well correlated. In contrast, the model computes latent heat

flux based on bulk formulae, so the good agreement with TropFlux is encouraging. Though sensible and longwave fluxes have lower correlations, they represent only a small part of intraseasonal flux variability, so the modeled net heat flux has a correlation of 0.7 with TropFlux, significant above the 95 % level. We also used the TropFlux wind product to validate the reanalysis winds that were used to force the model (not shown). At all longitudes across the equatorial Pacific, the correlation between reanalysis and TropFlux winds exceeds 0.85 for both the unfiltered and intraseasonal signals. Within the warm pool, the model winds are about 5–10 % weaker than those from TropFlux. This comparison assures us that the wind forcing used to drive the model is accurate, including at the intraseasonal timescale.

Finally, we validated the modeled upper ocean currents against in situ observations from the TAO moorings along the equator. Daily zonal currents from both the model output and available TAO sensors were averaged over the top 40 m. Table 2 shows the correlation, regression, and relative variance between modeled and observed currents at each equatorial mooring location, for both unfiltered and intraseasonal data. In the western Pacific Ocean (west of 170°W), the model does an excellent job of reproducing both filtered and unfiltered ocean currents, with correlations exceeding 0.7 and 0.8, respectively. Correlations for intraseasonal signals decrease substantially from the

Fig. 4 Validation of modeled SST: **a** raw model output, and **(b)** TMI daily gridded SST (for overlapping time period). *Thick black line* denotes the edge of the warm pool, defined by the 29 °C isotherm. **c** Correlation coefficient, R , at each longitude between model and observed SSTs: *black* is for the raw data (i.e. **a** and **b**), *grey* is for the intraseasonal (TIWs removed) anomalies. **d** Regression coefficient, κ , between the model output and observed SSTs, with values >1 indicating the model value is greater than the observation. **e** Intraseasonal anomalies of the WPEE as calculated from the model output (*black*) and from TMI observations (*red*); correlation $R = 0.91$. The statistical comparisons were made using model output and observations from January 1998 to December 2008. Both model and observations were averaged from 2°S to 2°N. Note that the year labels on the *y-axis* of **(a)** and **(b)** refer to January 1



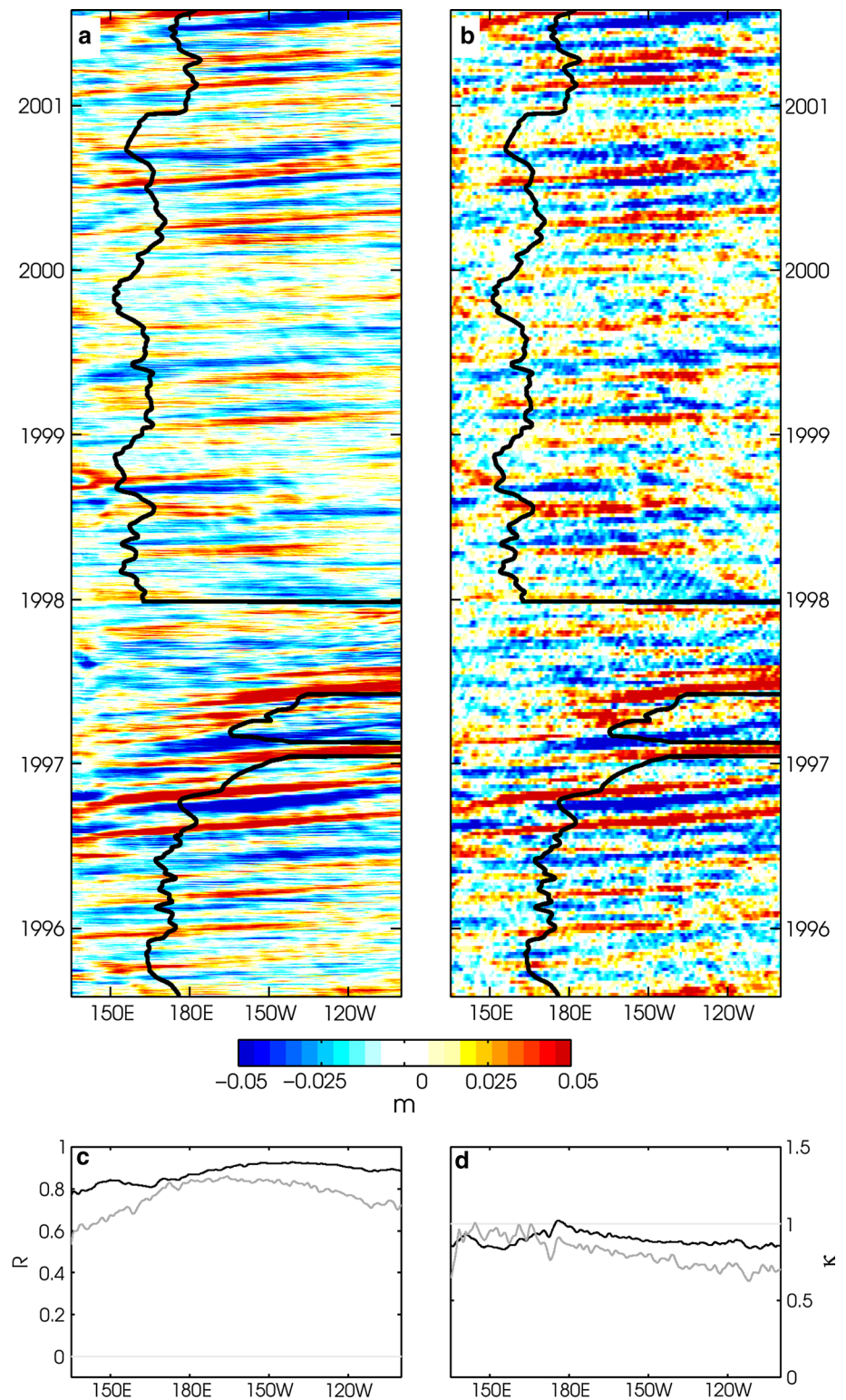
dateline, reaching $R = 0.24$ at 110° W. This is likely due to the large TIW signal in the eastern Pacific Ocean. TIWs are the result of internal oceanic instabilities, and we do not expect to reproduce their observed phase in a forced OGCM simulation. Furthermore, we cannot easily filter out the TIW signal from TAO data, given the relatively large distance between adjacent TAO moorings. Lower correlations between TAO and modeled intraseasonal currents in the eastern Pacific are thus likely to result from the superposition of TIW-induced “noise” and wind-forced surface current “signal”.

4 Driving mechanisms of intraseasonal variability at the WPEE

4.1 Dynamics over the equatorial Pacific Ocean

Figure 6a shows the contributions of heat flux forcing, zonal and meridional advection, and vertical processes to intraseasonal variations of SST at each longitude, calculated by regressing each term on the right-hand side of Eq. 1 to the temperature tendency on the left-hand side of Eq. 1. Recall that TIWs have been filtered out from

Fig. 5 Validation of SLA. As for Fig. 4a–d, but showing intraseasonal anomalies of SLA, (a) from the model, and (b) from the Aviso gridded 7-day product. (c) and (d) show the correlation and regression coefficients, respectively, computed over the equatorially-averaged unfiltered (*black*) and intraseasonal (*grey*) signals for October 1992 to December 2008, where the model output has been subsampled to the same 7-day grid as the observations and both model and observations were averaged from 2°S to 2°N



the tendency terms, so the results are representative of forced rather than internally generated intraseasonal variations. The results are consistent with previous studies: in the western Pacific, heat flux dominates intraseasonal SST variations, accounting for 50–80 % of the temperature

tendency west of the dateline (e.g., Hendon and Glick 1997; Drushka et al. 2012). Latent heat flux anomalies account for two thirds of intraseasonal net heat flux variations over the western Pacific, with shortwave fluxes contributing nearly all of the rest (not shown). The contribution

of heat flux drops steadily toward the central Pacific Ocean, while that of the other terms increases: by around 170°W the combined zonal and meridional advection account for more of the temperature variations than does heat flux. At

Table 1 Breakdown of modeled heat flux components, and validation of flux data against the TropFlux product

Flux component	Percentage of net (%)	Correlation	Regression coefficient
Shortwave	31	0.95	1.1
Latent	66	0.81	0.66
Sensible	4	0.49	0.44
Longwave	-2	0.66	0.43
Net	100	0.70	0.66

Statistics are calculated based on intraseasonal flux anomalies averaged over $\pm 2^\circ\text{C}$ longitude of the WPEE, for the 1984–2008 time period

Table 2 Validation of modeled upper ocean (averaged over the top 40 m) zonal currents

Mooring	N	Correlation coefficient		Regression coefficient		Relative variance	
		Raw	Intraseas.	Raw	Intraseas.	Raw	Intraseas.
147E	3,338	0.82	0.74	0.77	1	0.8	1
156E	1,006	0.85	0.73	0.81	0.85	0.82	0.89
165E	4,995	0.85	0.75	0.83	0.82	0.86	0.86
170W	5,412	0.75	0.63	0.76	0.74	0.81	0.83
140W	5,709	0.74	0.45	0.51	0.47	0.6	0.69
110W	5,321	0.67	0.24	0.42	0.18	0.54	0.55

Comparisons were made between observations from TAO moorings along the equator and model output subsampled to each mooring location, using all dates between 1990 and 2008 for which there were mooring data (number of days given by N). Each statistic was computed for both raw (unfiltered) and intraseasonally-filtered data

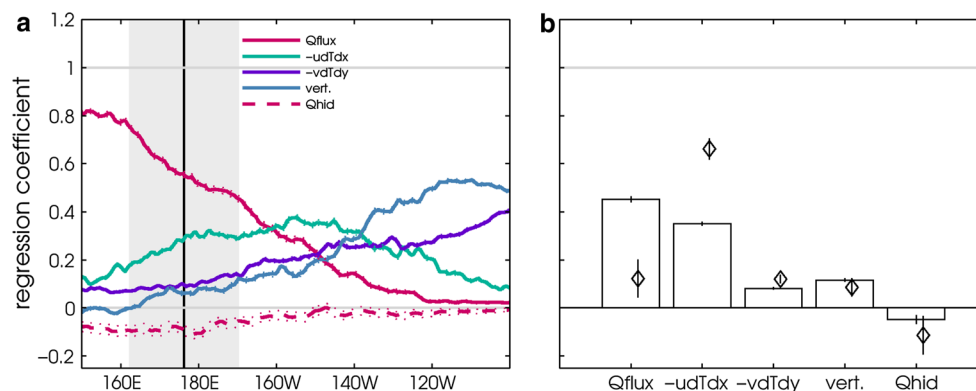


Fig. 6 Intraseasonal heat budget regressions. **a** Each color represents the contribution of a given term on the right-hand side of Eq. 1 to the intraseasonal mixed-layer temperature tendency (left-hand side of Eq. 1) along the equator in the Pacific Ocean: heat flux forcing (pink), zonal heat advection (green), meridional heat advection (purple), vertical processes (blue), and the hidden relaxation term (pink-dashed). **b** regression coefficients, where only the data at the longitude of the WPEE at any given time have been used to compute the regressions. The bars show the contribution of each term to the intraseasonal bal-

around 160° W, zonal advection dominates the intraseasonal heat budget (e.g., McPhaden 2002). In the eastern-most part of the basin, vertical diffusion and entrainment and meridional advection dominate, as has been previously observed (e.g., Halkides et al. 2011, though note that this paper included TIWs whereas we have removed TIWs and so consider only forced intraseasonal dynamics). The hidden relaxation term, Q_{hid} , accounts for less than 7 % of the signal (Fig. 6a), indicating that it does not heavily bias intraseasonal variations in modeled mixed-layer temperature (see Sect. 2.1 for a description of how this was calculated).

Based on the position and variability of the WPEE shown in Fig. 6a, there are several processes that can potentially contribute to intraseasonal SST variations at the edge of the warm pool: in the western-most range of the WPEE (i.e., warm pool trapped to the far western Pacific), heat

ance using data at all times; the diamonds show only the contribution associated with the WPEs considered in this study. Regressions were computed using model output from 1984 to 2008, averaged from 2°S to 2°N. In (a) the horizontal axis indicates longitude and the vertical line (shading) indicate the mean (standard deviation) WPEE based on the 29 °C isotherm. In (b) the vertical lines denote the standard error on each regression, which is taken to be the uncertainty. Note that TIWs have been filtered out from all terms, so the regressions represent other intraseasonal variations

flux accounts for nearly 80 % of intraseasonal mixed-layer temperature variability and zonal advection 25 %; at the eastern-most range, they contribute nearly equally (35 and 30 %, respectively).

4.2 Dynamics near the edge of the warm pool

Here, we show that intraseasonal displacements of the WPEE can be estimated based on local intraseasonal SST variations divided by the local zonal SST gradient. If the longitude of the WPEE, W , is defined by an isotherm, then the local variation of mixed-layer temperature at the edge of the warm pool should be related to the speed at which W varies and the local temperature gradient:

$$\partial_t \mathcal{T}|_W = (-\partial_t W)(\partial_x \mathcal{T}|_W), \quad (4)$$

where the negative sign accounts for the fact that upper ocean temperature decreases from west to east in the Pacific Ocean. Equation 4 can be decomposed into background (denoted with an over-bar) and intraseasonal (denoted with a prime symbol) components in order to diagnose intraseasonal variations in WPEE:

$$(\partial_t \mathcal{T}|_W)' = -(\overline{\partial_t W})(\partial_x \mathcal{T}|_W)' - (\partial_t W)'(\overline{\partial_x \mathcal{T}|_W}) - (\partial_t W)'(\partial_x \mathcal{T}|_W)'. \quad (5)$$

We assume intraseasonal variations in zonal SST gradient are negligible compared to the background gradient ($\overline{\partial_x \mathcal{T}} \gg \partial_x \mathcal{T}'$), and rearrange Eq. 5 to give the approximation

$$(\partial_t W)' \sim -\frac{\partial_t \mathcal{T}'|_W}{\partial_x \mathcal{T}|_W}. \quad (6)$$

We assess whether this relationship holds true by plotting the temporal derivative of the WPEE longitude at each time against the temporal derivative of intraseasonal SST at the WPEE scaled by the background (interannual + seasonal) zonal SST gradient at the WPEE. Data-points for which the denominator of Eq. 6 was near zero were removed to avoid the expression blowing up (51 points removed out of 9125). The high correlation ($R = 0.80$, significant at the 99 % confidence level) between the left- and right-hand sides of Eq. 6 (Fig. 7) illustrates that most intraseasonal variations in WPEE can be explained by intraseasonal temperature changes at the WPEE acting on the local background SST gradient. Note that when intraseasonal variations in zonal SST gradient were used in place of the background gradients (i.e. $\partial_x \mathcal{T}'|_W$ in place of $\overline{\partial_x \mathcal{T}|_W}$; not shown), correlations were negligible, illustrating that the background zonal temperature gradient is an important oceanic preconditioning for intraseasonal warm pool excursions and validating our a priori assumption that intraseasonal variations in the SST gradient, though occasionally large, are not

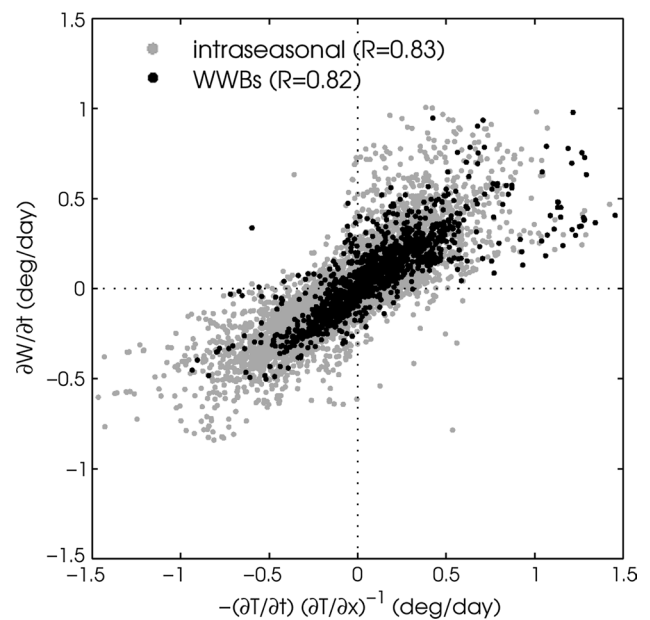
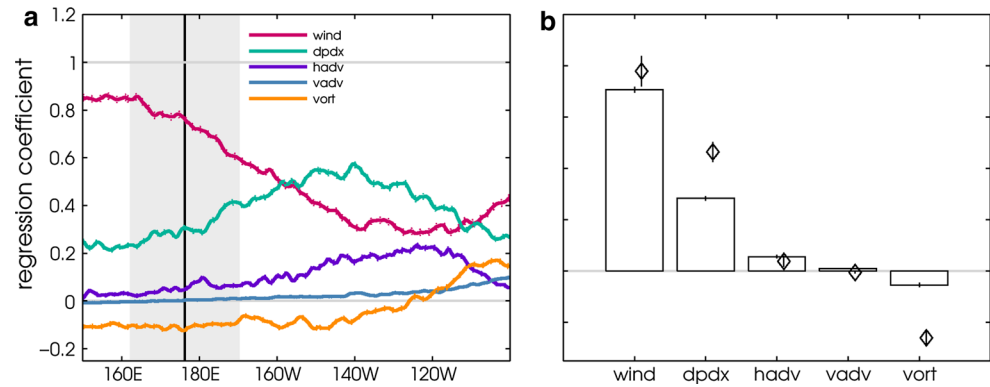


Fig. 7 Scatterplot of left- versus right-hand side of Eq. 6, where each data point is taken at the longitude of the WPEE at a given time. The grey data points are for all days from 1984–2008 (correlation, R , of 0.83), and the black data points are only for data in the 10 days following WWEs ($R = 0.82$)

important for dynamics at the WPEE and can reasonably be neglected.

To understand what causes the observed intraseasonal variations in temperature at the WPEE, we revisit the heat budget analysis shown in Fig. 6a, but rather than performing the regressions at each separate longitude, we only use the points along the WPEE; that is, for a given time t_i , we take the longitude of the WPEE $x_i = W(t_i)$ and extract each of the intraseasonal-anomaly heat budget terms in Eq. 1, $X'(x_i, t_i)$, which we denote $X'(t_i)|_W$. We then regress each term on the right-hand side of Eq. 1, $X'(t)|_W$, to the intraseasonal temperature tendency at the WPEE, $(\partial_t \mathcal{T}|_W)'$, to estimate the average contribution of each term in the heat budget to intraseasonal temperature anomalies right at the WPEE. Although numerous studies have shown that intraseasonal heat fluxes dominate temperature anomalies *within* the warm pool (e.g., Shinoda et al. 1998), their role *at the edge* of the warm pool—that is, driving oscillations in warm pool extent—has generally been overlooked. We find that anomalous heat fluxes drive intraseasonal temperature variations at the edge of the warm pool, accounting for 45 % of the observed $(\partial_t \mathcal{T}|_W)'$, with intraseasonal zonal heat advection contributing 37 % (Fig. 6b). Vertical advection and diffusion account for 8 % of the temperature anomaly and meridional advection ~8%. The “hidden” relaxation term contributes less than any other term, suggesting that there is no significant, systematic model bias that affects thermodynamics at the WPEE. Note that in Fig. 7 we relate motions of the WPEE to $\partial_t \mathcal{T} / \partial_x \mathcal{T}$, whereas

Fig. 8 As for Fig. 6, but for the momentum budget (Eq. 2), showing the contributions to zonal momentum from wind stress forcing (*pink*), pressure gradient forcing (*green*), horizontal momentum advection (*purple*), vertical momentum advection (*blue*), and planetary vorticity (*yellow*)



in Fig. 6b we explain variations in $\partial_t \mathcal{T}$; since intraseasonal variations in $\partial_x \mathcal{T}$ are small, these are equivalent.

To understand which processes drive the horizontal heat advection at the WPEE (and hence 37 % of intraseasonal WPEE excursions), we examine the surface momentum budget. First, we consider the momentum budget at all longitudes throughout the equatorial Pacific Ocean (Fig. 8a, bars). Zonal wind stress forcing completely dominates the intraseasonal momentum budget throughout the western and central part of the basin, with 80 % of the signal in the far west (which is the primary forcing region for intraseasonal variability); zonal pressure gradient force accounts for roughly 20 %, and advection and Coriolis acceleration are each <5 %. Further east, the relative importance of wind stress drops while the pressure gradient becomes as important as the wind stress forcing. This is consistent with the intraseasonal SLA signal, which shows the most energetic intraseasonal anomalies between around 180° E and 150° W (Fig. 5a, b). Only in the far eastern Pacific are Coriolis acceleration or vertical processes non-negligible.

Momentum budget regressions in the frame of the WPEE show that local intraseasonal wind forcing accounts for most (~73%) of the zonal momentum flux right at the WPEE (Fig. 8b, bars). The zonal pressure gradient accounts for 28 %, horizontal advection less than 6 %, and vorticity -8 %; vertical advection is negligible. In other words, despite strong intraseasonal Kelvin wave activity in the vicinity of the WPEE (Fig. 5a, b), local momentum input from winds dominates intraseasonal velocity variations there.

5 Driving mechanisms of intraseasonal variability at the WPEE related to WWEs

The implication of the bars plotted in Fig. 6b is that, on average, intraseasonal anomalies in temperature at the warm pool edge—and thus intraseasonal WPEE excursions—are caused by local heat flux variations. Although this is not a surprising finding when considered from the

perspective of Fig. 6a, which clearly shows that heat fluxes dominate at the longitudes spanned by the WPEE, it differs from previous studies that have only considered the role of strong zonal advection related to Kelvin wave processes in the central Pacific Ocean near the WPEE (e.g., Kessler et al. 1995; McPhaden 1999, 2002). To reconcile this discrepancy, we now focus on the WPEE displacements that are related to WWEs.

When only WWEs are considered, there remains a strong relationship between WPEE speed ($\partial W/\partial t$) and anomalous temperature at the WPEE (Fig. 7), which motivates examining the heat budget related to WWEs alone in order to understand how WWEs drive intraseasonal WPEE displacements. Figure 9 shows composites of the intraseasonal anomalies of different variables associated with WWEs (see Sect. 2 for details about how the WWEs were extracted). We are interested in the impacts of the westerly wind events on the WPEE, so we center the reference frame on the (time, longitude) that the Kelvin wave intersects the WPEE following each WWE (i.e. square markers in Fig. 3) and then average across the set of 114 WWEs. The average WWE is strongest (composite amplitude exceeding 0.02 N m^{-2}) around 10 days earlier and 20° west of the intersection of the Kelvin wave with the WPEE (Fig. 9a). The average wind stress anomaly extends eastward from its peak, leading to significant positive wind stress at the longitude of the WPEE for ~10 days before the Kelvin wave arrival. We will later show that this contributes to local momentum forcing at the WPEE. The WWE drives a Kelvin wave and a strong eastward surface jet: the Kelvin wave signal is clearly visible as a positive sea level anomaly that propagates eastward from the WWE with an average phase speed of $\sim 2.8 \text{ m s}^{-1}$ (Fig. 9b). Zonal currents exceeding 0.25 m s^{-1} arise just beneath the WWE and propagate eastward along with the Kelvin wave (Fig. 9d). A SST anomaly develops 10°–15° west of the WPEE a few days before the Kelvin wave arrival, and persists for 25–30 days (Fig. 9c): this warming is responsible for shifting the WPEE eastward (typically a 0.2° C warming causes an eastward WPEE displacement of a few degrees).

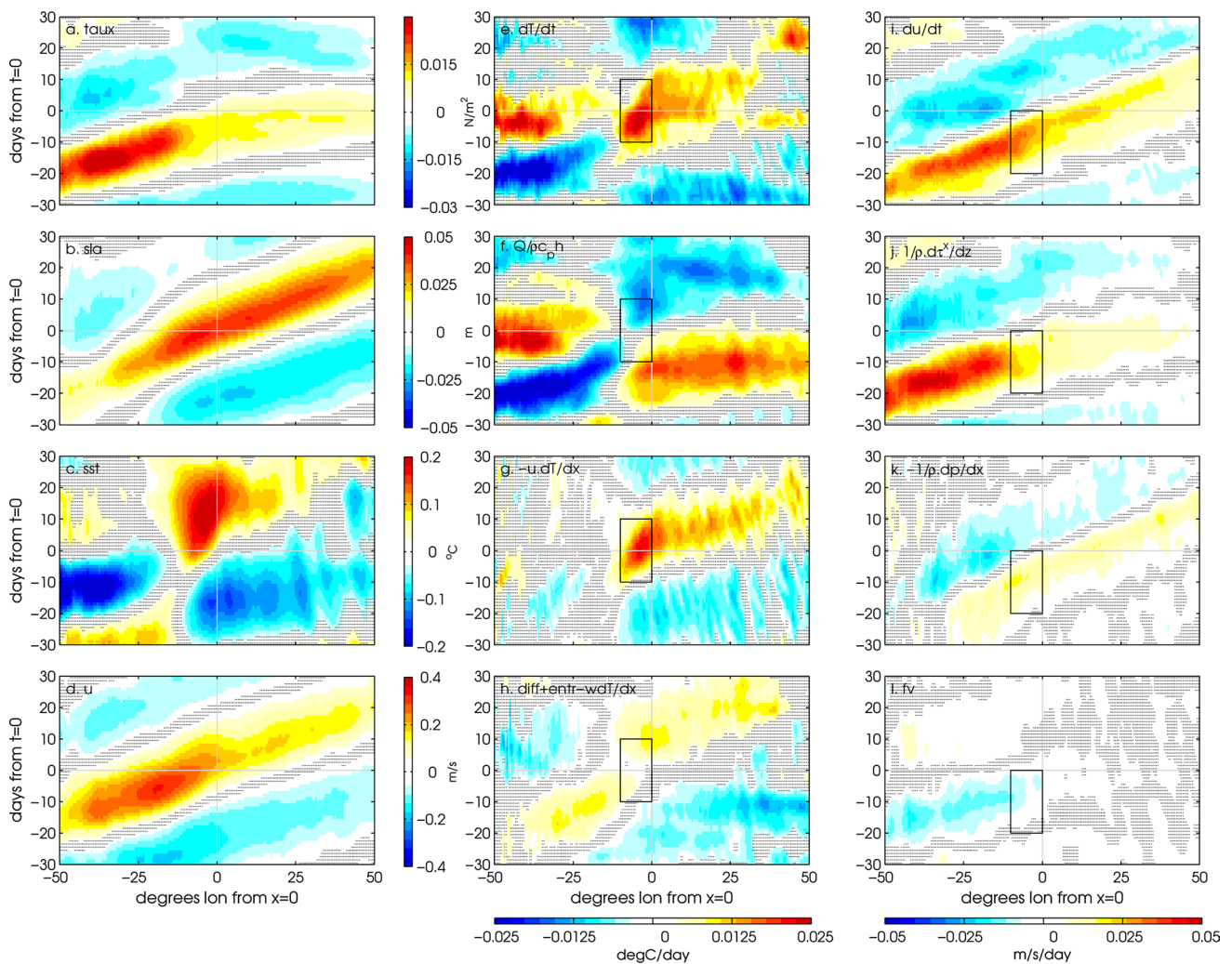


Fig. 9 Composites of intraseasonal anomalies associated with WWEs ($N = 114$). **(a)** zonal wind stress; **(b–d)** upper ocean response: SLA, SST, and surface current; **(e–h)** mixed-layer heat budget terms (Eq. 1): temperature tendency, heat flux forcing, zonal heat advection, and vertical terms); **(i–l)** mixed-layer momentum budget terms (Eq. 2): surface acceleration, zonal wind forcing, zonal pressure gradient forcing, and the Coriolis term. The composites are centered at the intersection of the Kelvin wave path and the WPEE (square markers in Fig. 3); that is, for a given WWE, $t = 0$ refers to the time that the associated Kelvin wave intersects the WPEE,

Composites of the individual terms in the heat and momentum budgets (Eqs. 1 and 2) reveal that the processes responsible for SST and zonal velocity anomalies associated with WWEs are very different than those responsible for the average intraseasonal anomalies at the WPEE that are shown as bars in Figs. 6b and 8b. Whereas heat flux anomalies drive the average temperature change at the WPEE (Fig. 6b), the spatio-temporal pattern of WWE-related warming at the WPEE (Fig. 9e) closely resembles that of horizontal heat advection (Fig. 9g), suggesting that zonal heat advection drives temperature changes following

and $x = 0$ refers to the longitude of the WPEE at that time. Stippled regions indicate the composites are not statistically significant (mean $<$ standard error). The black rectangles in the heat and momentum budget panels (**e–h** and **i–l**) indicate the area over which averages were computed in order to estimate the respective momentum and heat budget regressions associated with WWEs: 5° longitude west of the WPEE; and 10 days before and after (20 days before) the Kelvin wave-WPEE intersection for the heat (momentum) terms, reflecting the fact that we are interested in which processes drive local temperature changes, with a focus on what drives zonal advection

WWEs and thus eastward displacements of the warm pool. In fact, although heat flux anomalies at the WPEE are positive prior to the Kelvin wave arrival, they are negative afterward and thus act to reduce the warming at the WPEE. Diffusion and vertical advection and entrainment contribute weakly to the warming signal (Fig. 9h). Meridional heat advection also produces warming at the WPEE (not shown).

Composite averages of the zonal momentum terms reveal that Kelvin wave-induced geostrophic velocity anomalies, though large, are less important than local wind

forcing at the WPEE (Fig. 9i–k). Even accounting for the fact that the model underestimates the amplitude of intraseasonal SLA at the WPEE by $\sim 8\%$ (Fig. 5d), and thus may underestimate the contribution of zonal pressure gradient forcing, local wind stress still dominates the signal. This is a somewhat surprising result, as most previous studies looking at the impacts of WWEs on the WPEE have concentrated on the role of Kelvin wave-induced geostrophic velocity anomalies (e.g., Kessler et al. 1995; Picaut and Delcroix 1995; Delcroix and Dewitte 2000). While the importance of WWEs for generating local momentum anomalies has been shown with observations (Feng et al. 2005), to our knowledge this has not been tied to WPEE motions.

The composites provide a picture of how the upper ocean responds, on average, to forcing from WWEs; we quantify this more precisely by performing a regression analysis similar that done for the intraseasonal data along the entire WPEE, but for data related to the WWEs only. The choice of how to best quantify the thermodynamic impacts of WWEs is somewhat arbitrary. Since our objective is to understand how much each term in the heat budget contributes to intraseasonal SST anomalies at the WPEE following each wind event, we average spatially over 5°C of longitude west of the longitude of the WPEE–Kelvin wave intersection, and temporally integrate over the ± 10 days surrounding the time of the intersection (rectangle in Fig. 9e–h). This corresponds to the time period over which the SST change is largest (Fig. 9e). This gives one data-point per WWE for each term in Eq. 1; we then perform a linear regression between each of the terms on the right-hand side of the equation and the temperature tendency on the left-hand side (as was done for all times to form the intraseasonal regressions). Note that although the exact values of the regression coefficients depend on the choice of time and space over which we integrate, the general findings are independent of the choice. The regression coefficient for each term in the heat budget is shown as a diamond-shaped marker in Fig. 6b. Comparing the regression coefficients for WWEs with those for the intraseasonal anomalies (bars in Fig. 6b), it is clear that although WWEs are considered intraseasonal features and the two are often not explicitly distinguished, their dynamics are profoundly different. Following WWEs, the heat flux contribution to SST anomalies at the WPEE is around 15% , compared to 45% for all intraseasonal variations. The heat flux signal is dominated by solar radiation anomalies; longwave and latent heat fluxes oppose the solar flux but are much smaller in magnitude (not shown). On the other hand, zonal heat advection produces 64% of the warming at the WPEE following WWEs compared to only 37% for all intraseasonal signals. Meridional heat advection contributes around 12% , and vertical processes around 10% .

With zonal heat advection so strongly dominating the WWE-related SST changes, the question of what drives the intraseasonal zonal surface jets becomes particularly important. The composites show that directly beneath the WWEs, wind stress dominates momentum anomalies, whereas the zonal pressure gradient (i.e. Kelvin waves) dominates the signal to the east of the WPEE. Right at the WPEE, both terms appear important (Fig. 9i–k). To quantify this more explicitly, we computed a momentum budget regression analysis for WWEs only, in a similar manner as for the heat budget (Fig. 6b). Since we are interested in what drives the velocity anomalies at the WPEE at the time that the Kelvin wave arrives, we integrated each term for each WWE over the 20 days before the Kelvin wave intersects the WPEE (rectangle in Fig. 9i–l), corresponding to the strongest momentum anomaly (Fig. 9i). The regressions reveal that while the zonal pressure gradient is far more important when only WWEs are considered (as compared to when all intraseasonal anomalies are considered), wind forcing at the WPEE still dominates the local zonal momentum anomalies (Fig. 8b). WWE-related winds contribute around 80% of the momentum at the WPEE, compared to 47% from zonal pressure gradient forcing (Table 3), though note that because the model in fact underestimates the intraseasonal SLA signal by $\sim 8\%$ (Fig. 5d), Kelvin waves may contribute somewhat more than 47% of the signal. Previous studies have generally attributed WWE-related eastward jets in the vicinity of the WPEE to Kelvin waves alone (e.g., McPhaden 1999); we suggest that Kelvin waves are indeed important drivers of zonal jets, but that the role of local wind anomalies at the WPEE along the wave path is equally important, if not more so.

Boulanger et al. (2001) and Lengaigne et al. (2002) showed that a WWE can drive an eastward jet via strong nonlinear horizontal momentum advection at the WPEE; we find this to be the true in some individual cases (not shown), but on average this term makes up only 2% of the signal. Feng et al. (2005) emphasized the importance of the Coriolis term in generating WWE-related negative momentum anomalies in the warm pool region; indeed, we find that the contribution of vorticity is -31% , compared to a small component (-8%) in the intraseasonal average.

6 Discussion

6.1 Summary

We use 25 years of output from a forced OGCM to assess intraseasonal dynamics at the edge of the western Pacific warm pool in order to assess the mechanisms that drive intraseasonal displacements of the WPEE, which may play a role in the onset of El Niño events. The model is shown to

accurately reproduce observed intraseasonal anomalies in sea level, WPEE displacement, and zonal surface currents in the western and central Pacific Ocean. We identify 114 intraseasonal WWEs. A comparison of heat and momentum budgets for all intraseasonal anomalies at the WPEE versus for just those anomalies associated with WWEs reveals two novel findings. First, average intraseasonal fluctuations in the temperature at the edge of the warm pool are caused primarily by local variations in net heat flux. This shows that intraseasonal heat fluxes are important not only for driving SSTs within the warm pool, as has been shown by many previous studies, but also for controlling the zonal extent of the warm pool. On the other hand, when only WWEs are considered, warming at the WPEE, and hence eastward displacement of the warm pool, is dominated by anomalies in zonal heat advection.

Second, we find that momentum at the WPEE, both for all intraseasonal anomalies and for those following WWEs, is driven primarily by zonal wind stress anomalies. This is in contrast to previous studies, which have usually focused on velocity anomalies excited by intraseasonal Kelvin waves. Our results show that while Kelvin waves do drive eastward jets, their impacts are strongest east of the warm pool; right at the WPEE, local wind forcing dominates intraseasonal momentum.

6.2 Limitations and uncertainties

As described in Sect. 2.1, the model uses a specified air temperature and humidity rather than adjusting them based on SST, which leads to uncertainties in the temperature and tendency terms; an estimate of this “hidden relaxation”

term, denoted Q_{hid} , provided an uncertainty on the heat budget. For all analyses performed, the magnitude of this term was smaller than any other term, and is hence unlikely to have influenced the conclusions reached here.

Because our analysis is based on dynamics right at the WPEE, it is important to understand the sensitivity to how the WPEE is defined. We defined the WPEE using the 29 °C isotherm; a warmer isotherm would shift the WPEE further west, where intraseasonal forcing from winds and heat flux are stronger (e.g., Fig. 2) and zonal SST gradients are weaker (Fig. 4a, b). Conversely, a cooler isotherm would result in a WPEE that is further east, where wind stress and heat fluxes are weaker, the SST gradient is stronger, and intraseasonal Kelvin waves are more coherent (Fig. 5a, b). Table 3 shows regression coefficients for terms in both the heat and momentum budgets using three different isotherms to define the WPEE, for intraseasonal variations at the WPEE as well as for WWE-related anomalies only (i.e. bar plots and diamonds, respectively, in Figs. 6b and 8b). The intraseasonal regressions are not sensitive to the choice of WPEE: regardless of the WPEE definition, heat flux drives intraseasonal SST anomalies at the WPEE and wind stress drives momentum anomalies. The heat budget associated with WWEs shows slightly more sensitivity to the WPEE definition: when the 28.5 °C isotherm is used, net zonal advection still dominates but heat flux contributes significantly to SST variations at the WPEE, whereas otherwise the heat flux contribution is small. Composites similar to Fig. 9 (not shown) reveal that this is the case not because the magnitude of intraseasonal heat fluxes is stronger at the 28.5 °C isotherm, but because all terms are substantially weaker, particularly zonal heat advection, so heat fluxes

Table 3 Regression coefficients for the heat and momentum balances for both intraseasonal anomalies at the WPEE and for WWE-related anomalies

	$\theta = 28.5\text{ }^{\circ}\text{C}$		$\theta = 29\text{ }^{\circ}\text{C}$		$\theta = 29.4\text{ }^{\circ}\text{C}$		$\theta = [28.529.4]\text{ }^{\circ}\text{C}$	
	Intraseas.	WWEs	Intraseas.	WWEs	Intraseas.	WWEs	Intraseas.	WWEs
<i>Heat balance</i>								
Heat flux	0.45	0.13	0.45	0.15	0.49	0.09	0.50	0.16
Zonal advec.	0.35	0.66	0.37	0.64	0.27	0.65	0.30	0.67
Meridional advec.	0.08	0.12	0.08	0.12	0.08	0.15	0.08	0.10
Vertical processes	0.12	0.08	0.10	0.09	0.16	0.12	0.12	0.06
<i>Momentum balance</i>								
Wind stress	0.71	0.77	0.73	0.82	0.64	0.7	0.79	0.751
Pressure gradient	0.28	0.47	0.28	0.47	0.35	0.48	0.26	0.50
Horizontal advec.	0.06	0.04	0.06	0.02	0.06	-0.03	(0.01)	(0.02)
Vertical processes	(0.01)	(-0.01)	(0.01)	(-0.01)	0.02	(0)	(0.01)	(-0.01)
Coriolis	-0.06	-0.26	-0.08	-0.31	-0.07	-0.20	-0.07	-0.25

Statistics calculated using four different definitions of the WPEE are presented: for the first three columns, WPEE is based on the longitude of an isotherm θ ; for the last column, WPEE is defined as the longitudes between the 28.5 and 29.4 °C isotherms. The second column corresponds to the values plotted in Figs. 6b and 8b. Values that are not statistically significant are in parentheses

account for a greater fraction of the smaller SST change. Similarly, zonal momentum advection following WWEs is weaker when the 28.5°C isotherm is used (Table 3). This demonstrates that within the commonly used range of WPEE definitions, the findings of our study are robust. In addition, we averaged data at each time between the longitudes corresponding to the 28.5 and 29.4°C isotherms and found similar values for the regression analysis, indicating that the findings of this study are not merely idiosyncrasies arising from considering dynamics at a single isotherm.

We also assess the sensitivity of the results to the filtering that was used to isolate the intraseasonal signal (7–120-day bandpass filter and removal of tropical instability waves via a frequency-wavelength decomposition; see Sect. 2.4). Within a reasonable range of cutoff frequencies for the bandpass filter (5–10 days cutoff for removing the fast variations, and 90–140 days for the interannual variations), we found the coefficients of the heat and momentum budget regressions to be within $\pm 10\%$ of the values presented here, indicating that our findings are not sensitive to the intraseasonal filtering window. Similarly, varying the filtering windows used to remove the TIWs did not significantly alter our findings. Supplementary Figure S1 shows composites constructed using data that were not filtered, but only had the time average over the ± 30 days from the relative origin of each WWE removed. This effectively removes the effects of interannual variability without imposing a particular time scale. Despite the lack of filtering, these closely resemble the composites based on filtered data that are shown in Fig. 9. The unfiltered composite averages are noisier, as the high-frequency signals have not been filtered out; this is particularly evident at positive relative longitudes, reflecting the influence of tropical instability waves. Comparing Fig. 9 (filtered data) with Supplemental Fig. S1 (unfiltered data) illustrates that the general features of the WWE composites are not artifacts of the filtering. However, energetic variations at frequencies outside the intraseasonal band (e.g., high-frequency and interannual variations, tropical instability waves) obscure the intraseasonal anomalies associated with WWEs, which motivates the use of a filter to remove variations on these timescales. We emphasize that we used the widest possible bandpass filter so as to avoid imposing a specific timescale of variability.

Much can be learned from model experiments forced with idealized WWEs (e.g., Giese and Harrison 1991; Fedorov 2002), which allow the potential pitfalls of intraseasonal filtering to be avoided. However, we also advocate the approach used here, of using a realistic model configuration that includes interannual variations. The response of the ocean to WWEs is sensitive to both the characteristics of the WWEs and the large-scale background atmosphere

and ocean conditions, so the simplest way to study what drives the ocean response to WWEs is to use a realistic model setup. In contrast, idealized experiments may not be adequate for tackling the full spectrum of possible combination of WWEs and background conditions, and the response may be sensitive to the details of the setup (especially the WWE-related wind signal at the eastern edge of the warm pool).

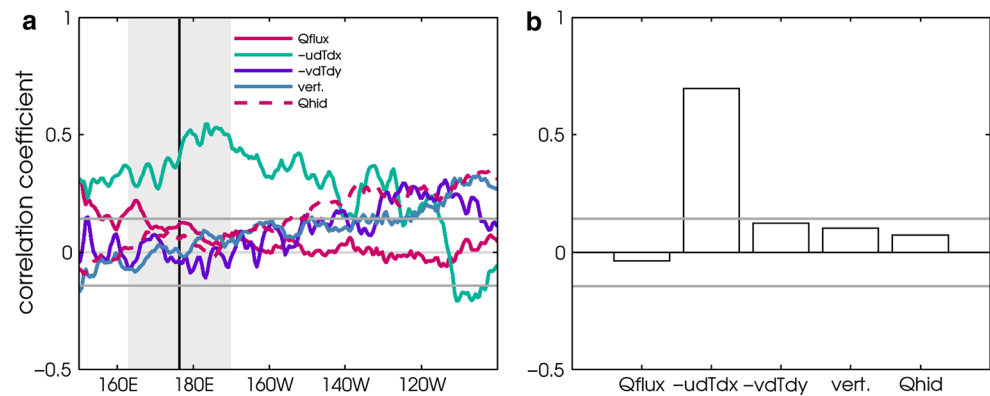
6.3 Comparison with interannual time-scales

On interannual timescales, zonal advection has been shown to clearly dominate excursions of the WPEE (Picaut et al. 1996). Indeed, a statistical analysis of the interannual mixed-layer heat balance at all longitudes reveals that only zonal heat advection is significantly correlated with interannual temperature variations in the western and central Pacific Oceans (Fig. 10a). In the eastern Pacific Ocean, all terms are weakly though significantly correlated with interannual temperature tendency, as has been shown previously (e.g., Zhang and McPhaden 2006). Similarly, in the reference frame of the WPEE, only zonal heat advection has a statistically significant correlation with the interannual temperature tendency (Fig. 10b), and hence with interannual excursions of the WPEE itself. Figure 10 confirms that that model behaves in a reasonable manner at interannual timescales, and highlights that intraseasonal and interannual processes near the WPEE are governed by very different dynamics.

6.4 Possible air–sea interactions at the WPEE and implications for ENSO

The findings of this study help to fill a gap in the literature regarding intraseasonal dynamics at the WPEE. It is well understood that heat flux drives intraseasonal SST variations within the warm pool (e.g., Hendon and Glick 1997; Shinoda et al. 1998), and zonal temperature advection dominates in the central Pacific Ocean (e.g., McPhaden 2002; Matthews et al. 2010); however, since the longitude of the WPEE varies dramatically on intraseasonal and interannual timescales, it is unclear what drives intraseasonal SST variations right at the edge of the warm pool. Past studies have focused on the role played by WWEs, which are found in the intraseasonal band but do not necessarily represent all intraseasonal variability. We have demonstrated that although WWEs are regarded as intraseasonal features, their impacts at the edge of the warm pool are distinct from average intraseasonal variability. Particularly striking is the result that although WWE-forced Kelvin waves contribute significantly to the surface jets seen at the WPEE, local wind stress anomalies appear to play an even more important role in driving these jets (Fig. 8b). This can be

Fig. 10 As for Fig. 6, but for interannual heat budget anomalies and showing correlation instead of regression coefficients. The *horizontal grey lines* in (a) indicate the 95 % significance level for the correlations. In (b) impacts of WWEs on interannual anomalies at the WPEE are not considered



understood by looking at the case of the March 1997 WWE shown in Fig. 3: the wind anomaly drives a Kelvin wave that propagates eastward from beneath the westerly wind event (Fig. 3b) and forces an eastward surface jet (Fig. 3d). SST warms in a 15° -wide band west of the WPEE beginning ~ 10 days after the strongest wind anomaly (Fig. 3b). At around the time and longitude that the Kelvin wave intersects the WPEE, a distinct westerly wind anomaly is seen (Fig. 3a), which contributes momentum locally to the jet. The composite wind stress forcing term (Fig. 9j) reveals a weakly positive wind anomaly around 15 days after the peak of the WWE, coinciding with the edge of the warm pool and contributing as much or more momentum to the eastward jet than does the Kelvin wave-related pressure gradient (Figs. 8b, 9k). This weaker wind anomaly at the WPEE could be the eastward tail of the primary westerly wind event. Alternatively, it could be a secondary westerly wind anomaly that is generated locally by the anomalously warm SSTs, a mechanism consistent with evidence suggesting that WWE-related warming at the WPEE can induce subsequent WWEs via air–sea coupling. For example, Latif et al. (1988), Lengaigne et al. (2003a), and Lengaigne et al. (2004b) used sensitivity tests with atmospheric and coupled general circulation models to demonstrate that a SST increase following a WWE causes an eastward shift of the ascending branch of the Walker circulation, which produces enhanced westerly wind activity following the initial westerly wind event. Tziperman and Yu (2007) used satellite observations to demonstrate that the large-scale Pacific Ocean SST structure affects the probability of occurrence, amplitude, location, and scale of WWEs. Results from these studies and others imply that WWEs are not fully stochastic processes, but instead are affected by the background SST. This has significant implications for ENSO. An observational case study by Yu et al. (2003) showed that WWE variability was enhanced when the warm pool was displaced eastward during the strong 1997–1998 El Niño event, and suppressed when the warm pool was displaced westward during the subsequent La Niña

in 1999–2000. The results of the present study therefore support the idea that coupled feedbacks between SST and WWEs are integral to ENSO dynamics (Lengaigne et al. 2003a; Eisenman et al. 2005; Gebbie et al. 2007).

Our study also reveals that WWEs are not the only atmospheric features responsible for WPEE displacements: indeed, intraseasonal WPEE fluctuations not related to WWEs were shown to be dominated by intraseasonal variations in net heat flux (Fig. 6b). Furthermore, when composites are formed based on events defined as intraseasonal WPEE displacements (e.g., eastward displacements exceeding 2° of longitude; see Sect. 3) it is clear that these “displacement events” are driven both by WWEs and by local anomalies in wind and heat flux at the WPEE (Supplementary Fig. S2e–g). While it is fairly well accepted that WWEs contribute to El Niño development (Lengaigne et al. 2004b; McPhaden 2004), our findings suggest that further study is needed in order to assess whether surface heat flux-induced zonal WPEE motions are strong enough to initiate the Bjerknes feedback and contribute to ENSO evolution. The question of what drives intraseasonal surface heat flux anomalies near the WPEE—for example, small-scale, local atmospheric disturbances versus large-scale atmospheric modes such as the MJO—also deserves further investigation.

6.5 Relationship to the Madden-Julian Oscillation

Though the MJO is probably one of the processes that generates WWEs (e.g., Zhang 2005), it is unclear if the MJO and WWEs have distinctive impacts on motions of the WPEE. To address this question, we sorted the data into active, suppressed, and neutral MJO conditions using the index of Wheeler and Hendon (2004), which is based on the first two empirical orthogonal functions of tropical convection and winds and is defined by an amplitude and a phase. We defined active conditions as having a phase of 6 or 7 and suppressed conditions as having a phase of 2 or 3, and limited both active and suppressed conditions

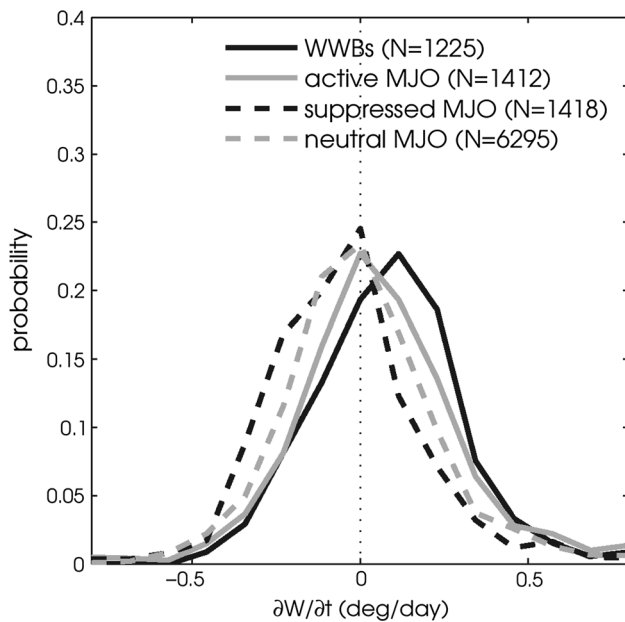


Fig. 11 Probability distribution function for time-derivative of WPEE displacement (i.e. y -axis in Fig. 7), for different conditions: only the 10 days following WWEs (black line); active MJO (grey); suppressed MJO (black dashed); and neutral MJO (grey dashed). MJO conditions are based on the Wheeler and Hendon (2004) index

to having an amplitude exceeding 1. All remaining times were designated as neutral MJO conditions. To characterize intraseasonal WPEE activity associated with these different conditions, we computed probability distributions for intraseasonal WPEE displacements ($\partial W/\partial t$; e.g. Fig. 7) for active, suppressed, and neutral MJO conditions as well as for WWEs only. Figure 11 illustrates that intraseasonal WPEE displacements associated with WWEs are shifted toward larger positive values, indicating that WWEs are linked to the strongest intraseasonal displacements of the WPEE and produce a net eastward shift of the WPEE. Interestingly, WPEE displacements for MJO active conditions are roughly symmetrical around zero, meaning that eastward intraseasonal WPEE displacement associated with MJO events is as likely as westward displacement, so the net displacement is likely near zero. During suppressed and neutral MJO conditions, WPEE displacements are skewed slightly toward negative values, so that the warm pool undergoes westward displacements when intraseasonal MJO-related winds and convection in the western Pacific Ocean are weak.

Figure 11 suggests that the ocean response to atmospheric forcing during MJO conditions may be distinctive from the response to WWEs. However, a more in-depth study of the mechanisms related to these differences is beyond the scope of this study.

Acknowledgments This work was supported by Agence Nationale de la Recherche (ANR) project METRO grant number 2010-BLAN-616-01. We gratefully acknowledge Benoît Vanni re and Christian Eth  for help with running the model, and S bastien Masson for useful feedback. We additionally thank three anonymous reviewers for their suggestions. Computations were carried out at the CNRS super-computing centre (IDRIS).

References

- Ashok K, Behera SK, Rao SA, Weng H, Yamagata T (2007) El Ni o Modoki and its possible teleconnection. *J Geophys Res* 112(C11)
- Baturin N, Niiler P (1997) Effects of instability waves in the mixed layer of the equatorial Pacific. *J Geophys Res* 102(C13):27771–27793
- Bjerknes J (1969) Atmospheric teleconnections from the equatorial Pacific 1. *Mon Weather Rev* 97(3):163–172
- Blanke B, Delecluse P (1993) Variability of the tropical Atlantic Ocean simulated by a general circulation model with two different mixed-layer physics. *J Phys Oceanogr* 23(7):1363–1388
- Bosc C, Delcroix T, Maes C (2009) Barrier layer variability in the western Pacific warm pool from 2000 to 2007. *J Geophys Res* 114(C6):C06023
- Boulanger J, Menkes C (1999) Long equatorial wave reflection in the Pacific Ocean from TOPEX/POSEIDON data during the 1992–1998 period. *Clim Dyn* 15(3):205–225
- Boulanger J, Durand E, Menkes C, Delecluse P, Imbard M, Lengaigne M, Madec G, Masson S (2001) Role of non-linear oceanic processes in the response to westerly wind events: new implications for the 1997 El Ni o onset. *Geophys Res Lett* 28(8):1603–1606
- de Boyer Mont gut C, Vialard J, Shenoi S, Shankar D, Durand F, Eth  C, Madec G (2007) Simulated seasonal and interannual variability of the mixed layer heat budget in the northern Indian Ocean. *J Clim* 20(13):3249–3268
- Brodeau L, Barnier B, Treguier A, Penduff T, Gulev S (2010) An ERA40-based atmospheric forcing for global ocean circulation models. *Ocean Modelling* 31(3–4):88–104
- Cronin M, McPhaden M (1997) The upper ocean heat balance in the western equatorial Pacific warm pool during September–December 1992. *J Geophys Res* 102:8533–8553
- Delcroix T, Dewitte B et al (2000) Equatorial waves and warm pool displacements during the 1992–1998 El Ni o Southern Oscillation events: Observation and modeling. *J Geophys Res* 105(C11):26,045–26
- Drushka K, Sprintall J, Gille S, Wijffels S (2012) In situ observations of Madden-Julian Oscillation mixed layer dynamics in the Indian and western Pacific Oceans. *J Clim* 25(7):2306–2328
- Ducet N, Le Traon P, Reverdin G (2000) Global high-resolution mapping of ocean circulation from TOPEX/Poseidon and ERS-1 and -2. *J Geophys Res* 105(C8):19,477–19,498
- Eisenman I, Yu L, Tziperman E (2005) Westerly wind bursts: ENSO’s tail rather than the dog? *J Clim* 18(24):5224–5238
- Farrar J (2011) Barotropic Rossby waves radiating from tropical instability waves in the Pacific Ocean. *J Phys Oceanogr* 41(6):1160–1181
- Fedorov AV, Hu S, Lengaigne M, Guilyardi E (2014) The impact of westerly wind bursts and ocean initial state on the development, and diversity of El Ni o events. *Clim Dynam* 1–21. doi:10.1007/s00382-014-2126-4
- Fedorov AV (2002) The response of the coupled tropical ocean-atmosphere to westerly wind bursts. *Q J R Meteorol Soc* 128(579):1–23
- Feng M, Lukas R, Hacker P, Plueddemann A, Weller R (2005) Upper ocean momentum balances in the western equatorial Pacific on the intraseasonal time scale. *Deep Sea Res Part I* 52(5):749–765

- Gebbie G, Eisenman I, Wittenberg A, Tziperman E (2007) Modulation of westerly wind bursts by sea surface temperature: a semi-stochastic feedback for ENSO. *J Atmos Sci* 64(9):3281–3295
- Gebbie G, Tziperman E (2009) Incorporating a semi-stochastic model of ocean-modulated westerly wind bursts into an ENSO prediction model. *Theor Appl Climatol* 97(1):65–73
- Giese BS, Harrison D (1991) Eastern equatorial Pacific response to three composite westerly wind types. *J Geophys Res* 96(S01):3239–3248
- Gill A (1980) Some simple solutions for heat-induced tropical circulation. *Q J R Meteorol Soc* 106(449):447–462
- Graham N, Barnett T (1987) Sea surface temperature, surface wind divergence, and convection over tropical oceans. *Science* 238(4827):657–659
- Halkides D, Lucas L, Waliser D, Lee T, Murtugudde R (2011) Mechanisms controlling mixed-layer temperature variability in the eastern tropical Pacific on the intraseasonal timescale. *Geophys Res Lett* 38(17):L17,602
- Harrison D (1984) The appearance of sustained equatorial surface westerlies during the 1982 Pacific warm event. *Science* 224:1099–1102
- Harrison D, Vecchi G (1997) Westerly Wind Events in the Tropical Pacific, 1986–95. *J Clim* 10(12):3131–3156
- Hendon H, Glick J (1997) Intraseasonal air–sea interaction in the tropical Indian and Pacific Oceans. *J Clim* 10(4):647–661
- Im SH, An SI, Lengaigne M, Noh Y (2012) Seasonality of tropical instability waves and its feedback to the seasonal cycle in the tropical Eastern Pacific. *Sci World J* 2012. doi:10.1100/2012/612048
- Jackett D, McDougall T (1995) Minimal adjustment of hydrographic profiles to achieve static stability. *J Atmos Oceanic Tech* 12(2):381–389
- Jiang C, Thompson L, Kelly K, Cronin M (2009) The roles of intraseasonal Kelvin waves and tropical instability waves in SST variability along the equatorial Pacific in an isopycnal ocean model. *J Clim* 22(12):3470–3487
- Keen R (1982) The role of cross-equatorial tropical cyclone pairs in the Southern Oscillation. *Mon Weather Rev* 110:1405–1415
- Keerthi M, Lengaigne M, Vialard J, de Boyer Montégut C, Muraleedharan P (2012) Interannual variability of the tropical Indian Ocean mixed layer depth. *Clim Dyn* 40(3–4):1–17
- Kessler WS (2005) The oceans. In: Lau WKM, Waliser DE (eds) *Intraseasonal variability in the atmosphere-ocean climate system*, Springer, Berlin, Heidelberg, pp 175–222
- Kessler W, McPhaden M, Weickmann K (1995) Forcing of intraseasonal Kelvin waves in the equatorial Pacific. *J Geophys Res* 100:10,613–10,632
- Kumar BP, Vialard J, Lengaigne M, Murty V, McPhaden M, Cronin M, Pinsard F, Reddy KG (2012a) TropFlux wind stresses over the tropical oceans: evaluation and comparison with other products. *Clim Dyn* 40(7–8):1–23
- Kumar P, Vialard J, Lengaigne M, Murty V, McPhaden M (2012b) TropFlux: air–sea fluxes for the global tropical oceans-description and evaluation. *Clim Dyn* 38:1521–1543
- Latif M, Biercamp J, Von Storch H (1988) The response of a coupled ocean-atmosphere general circulation model to wind bursts. *J Atmos Sci* 45(6):964–979
- Legeckis R (1977) Long waves in the eastern equatorial Pacific Ocean: a view from a geostationary satellite. *Science* 197(4309):1179–1181
- Lengaigne M, Boulanger J, Menkes C, Masson S, Madec G, Delecluse P (2002) Ocean response to the March 1997 westerly wind event. *J Geophys Res* 107(C12):8015
- Lengaigne M, Boulanger J, Menkes C, Madec G, Delecluse P, Guilyardi E, Slingo J (2003a) The March 1997 westerly wind event and the onset of the 1997/98 El Niño: understanding the role of the atmospheric response. *J Clim* 16(20):3330–3343
- Lengaigne M, Madec G, Menkes C, Alory G (2003b) Impact of isopycnal mixing on the tropical ocean circulation. *J Geophys Res* 108(C11):3345
- Lengaigne M, Boulanger JP, Menkes C, Delecluse P, Slingo J (2004a) Westerly wind events in the tropical Pacific and their influence on the coupled ocean-atmosphere system: a review. *Geophys Monogr Ser* 147:49–69
- Lengaigne M, Guilyardi E, Boulanger JP, Menkes C, Delecluse P, Inness P, Cole J, Slingo J (2004b) Triggering of El Niño by westerly wind events in a coupled general circulation model. *Clim Dyn* 23(6):601–620
- Lengaigne M, Menkes C, Aumont O, Gorgues T, Bopp L, André JM, Madec G (2007) Influence of the oceanic biology on the tropical Pacific climate in a coupled general circulation model. *Clim Dyn* 28(5):503–516
- Lengaigne M, Hausmann U, Madec G, Menkes C, Vialard J, Molines J (2012) Mechanisms controlling warm water volume interannual variations in the equatorial Pacific: diabatic versus adiabatic processes. *Clim Dyn* 38(5–6):1031–1046
- Locarnini R, Mishonov AV, Antonov JI, Boyer TP, Garcia HE, Baranova OK, Zweng MM, Johnson DR (2010) *World Ocean Atlas 2009*, p 184
- Lopez H, Kirtman BP (2013) Westerly wind bursts and the diversity of ENSO in CCSM3 and CCSM4. *Geophys Res Lett* 40(17):4722–4727. doi:10.1002/grl.50913
- Lopez H, Kirtman BP, Tziperman E, Gebbie G (2013) Impact of interactive westerly wind bursts on ccsm3. *Dynam Atmos Ocean* 59:24–51. doi:10.1016/j.dynatmoce.2012.11.001
- Lucas L, Waliser D, Murtugudde R (2010) Mechanisms governing sea surface temperature anomalies in the eastern tropical Pacific Ocean associated with the boreal winter Madden-Julian Oscillation. *J Geophys Res* 115(C5):C05,012
- Madec G (2008) NEMO ocean engine. Tech. rep., Institut Pierre-Simon Laplace (IPSL), Note du Pole de modélisation 27
- Maes C, Sudre J, Garçon V (2010) Detection of the eastern edge of the equatorial Pacific warm pool using satellite-based ocean color observations. *SOLA* 6:129–132
- Matthews A, Singhruck P, Heywood K (2010) Ocean temperature and salinity components of the Madden-Julian oscillation observed by Argo floats. *Clim Dyn* 35(7–8):1149–1168. doi:10.1007/s00382-009-0631-7
- McPhaden M, Picaut J (1990) El Niño-Southern Oscillation displacements of the western equatorial Pacific warm pool. *Science* 250(4986):1385–1388
- McPhaden MJ, Hayes SP (1991) On the variability of winds, sea surface temperature, and surface layer heat content in the western equatorial Pacific. *J Geophys Res* 96:3331–3342
- McPhaden M, Bahr F, Du Penhoat Y, Firing E, Hayes S, Niiler P, Richardson P, Toole J (1992) The response of the western equatorial Pacific Ocean to westerly wind bursts during November 1989 to January 1990. *J Geophys Res* 97(C9):14,289–14,303
- McPhaden M, Busalacchi A, Cheney R, Donguy J, Gage K, Halpern D, Ji M, Julian P, Meyers G, Mitchum G et al (1998) The Tropical Ocean-Global Atmosphere observing system: a decade of progress. *J Geophys Res* 103(C7):14,169–14
- McPhaden M (1999) Genesis and evolution of the 1997–98 El Niño. *Science* 283(5404):950
- McPhaden MJ (2002) Mixed layer temperature balance on intraseasonal timescales in the equatorial Pacific Ocean. *J Clim* 15(18):2632–2647
- McPhaden MJ (2004) Evolution of the 2002/03 El Niño. *Bull Am Meteorol Soc* 85(5):677–695
- Menkes C, Vialard J, Kennan S, Boulanger J, Madec G (2006) A modeling study of the impact of tropical instability waves on the heat budget of the eastern equatorial Pacific. *J Phys Oceanogr* 36(5):847–865
- Nidheesh A, Lengaigne M, Vialard J, Unnikrishnan A, Dayan H (2012) Decadal and long-term sea level variability in the tropical Indo-Pacific Ocean. *Clim Dyn* 41(2):1–22

- Nisha K, Lengaigne M, Gopalakrishna V, Vialard J, Pous S, Peter AC, F Durand SN (2013) Processes of summer intraseasonal sea surface temperature variability along the coasts of India. *Ocean Dyn Rev* 63(4):329–346
- Paulson C, Simpson J (1977) Irradiance measurements in the upper ocean. *J Phys Oceanogr* 7(6):952–956
- Picaut J, Delcroix T (1995) Equatorial wave sequence associated with warm pool displacements during the 1986–1989 El Niño-La Niña. *J Geophys Res* 100(C9):18,393–18
- Picaut J, Ioualalen M, Menkes C, Delcroix T, McPhaden M (1996) Mechanism of the zonal displacements of the Pacific warm pool: implications for ENSO. *Science* 274(5292):1486
- Picaut J, Masia F, Du Penhoat Y (1997) An advective–reflective conceptual model for the oscillatory nature of the ENSO. *Science* 277(5326):663–666
- Picaut J, Ioualalen M, Delcroix T, Masia F, Murtugudde R, Vialard J (2001) The oceanic zone of convergence on the eastern edge of the Pacific warm pool: a synthesis of results and implications for El Niño–Southern Oscillation and biogeochemical phenomena. *J Geophys Res* 106(C2):2363–2386
- Qiao L, Weisberg R (1995) Tropical instability wave kinematics: observations from the tropical instability wave experiment. *J Geophys Res* 100(C5):8677–8693
- Roullet G, Madec G (2000) Salt conservation, free surface, and varying levels: a new formulation for ocean general circulation models. *J Geophys Res* 105(C10):23,927–23
- Seiki A, Takayabu Y (2007) Westerly wind bursts and their relationship with intraseasonal variations and ENSO. Part I *Stat Mon Weather Rev* 135(10):3325–3345
- Shinoda T, Hendon H, Glick J (1998) Intraseasonal variability of surface fluxes and sea surface temperature in the tropical western Pacific and Indian Oceans. *J Clim* 11(7):1685–1702
- Shinoda T, Hendon H (2001) Upper-ocean heat budget in response to the Madden–Julian Oscillation in the western equatorial Pacific. *J Clim* 14(21):4147–4165
- Trenberth KE, Branstator GW, Karoly D, Kumar A, Lau NC, Ropelewski C (1998) Progress during TOGA in understanding and modeling global teleconnections associated with tropical sea surface temperatures. *J Geophys Res Oceans* 103(C7):14,291–14,324
- Tziperman E, Yu L (2007) Quantifying the dependence of westerly wind bursts on the large-scale tropical Pacific SST. *J Clim* 20(12):2760–2768
- Uppala S, Källberg P, Simmons A, Andrae U, Bechtold V, Fiorino M, Gibson J, Haseler J, Hernandez A, Kelly G et al (2005) The ERA-40 re-analysis. *Q J R Meteorol Soc* 131(612):2961–3012
- Vialard J, Delecluse P (1998) An OGCM study for the TOGA decade. Part II: barrier-layer formation and variability. *J Phys Oceanogr* 28(6):1089–1106
- Vialard J, Menkes C, Boulanger J, Delecluse P, Guilyardi E, McPhaden M, Madec G (2001) A model study of oceanic mechanisms affecting equatorial Pacific sea surface temperature during the 1997–98 El Niño. *J Phys Oceanogr* 31(7):1649–1675
- Vialard J, Jayakumar A, Gnanaseelan C, Lengaigne M, Sengupta D, Goswami B (2012) Processes of intraseasonal sea surface temperature variability in the Northern Indian Ocean during boreal summer. *Clim Dyn* 38:1901–1916
- Wang C, Picaut J (2004) Understanding ENSO physics: a review. *Geophys Monogr Ser* 147:21–48
- Wheeler M, Hendon H (2004) An all-season real-time multivariate MJO index: development of an index for monitoring and prediction. *Mon Weather Rev* 132:1917–1932
- Yu L, Rienecker M (1998) Evidence of an extratropical atmospheric influence during the onset of the 1997–98 El Niño. *Geophys Res Lett* 25(18):3537–3540
- Yu L, Weller R, Liu W (2003) Case analysis of a role of ENSO in regulating the generation of westerly wind bursts in the western equatorial Pacific. *J Geophys Res* 108(C4):3128
- Zhang Y, Rossow W, Lacis A, Oinas V, Mishchenko M (2004) Calculation of radiative fluxes from the surface to top of atmosphere based on ISCCP and other global data sets: refinements of the radiative transfer model and the input data. *J Geophys Res* 109(D19):D19,105
- Zhang C (2005) Madden–Julian Oscillation. *Rev Geophys* 43:1–36
- Zhang X, McPhaden MJ (2006) Wind stress variations and interannual sea surface temperature anomalies in the eastern equatorial Pacific. *J Clim* 19(2):226–241